

A Scalable Variational Bayes Approach for Fitting Non-Conjugate Spatial Generalized Linear Mixed Models via Basis Expansions

Jin Hyung Lee^a, Ben Seiyon Lee^{b,*}

^a*Purdue University, 250 N. University Street, West Lafayette, 47907, IN, United States*

^b*George Mason University, 4400 University Drive, Fairfax, 22030, VA, United States*

Abstract

Large spatial datasets with non-Gaussian responses are increasingly common in environmental monitoring, ecology, and remote sensing, yet scalable Bayesian inference for such data remains challenging. Markov chain Monte Carlo (MCMC) methods are often prohibitive for large datasets, and existing variational Bayes methods rely on conjugacy or strong approximations that limit their applicability and can underestimate posterior variances. We propose a scalable variational framework that incorporates semi-implicit variational inference (SIVI) with basis representations of spatial generalized linear mixed models (SGLMMs), which may not have conjugacy. Our approach accommodates gamma, negative binomial, Poisson, Bernoulli, and Gaussian responses on continuous spatial domains. Across 20 simulation scenarios with 50,000 locations, SIVI achieves predictive accuracy and posterior distributions comparable to Metropolis-Hastings and Hamiltonian Monte Carlo while providing notable computational speedups. Applications to MODIS land surface temperature and Blue Jay abundance further demonstrate the utility of the approach for large non-Gaussian spatial datasets.

Keywords: Variational Bayes, Spatial Statistics, Semi-Implicit Variational Inference, Basis Representation, Non-Gaussian Spatial Data

*Corresponding author. *Postal address:* 4400 University Drive, Fairfax, VA 22030, USA. *Email:* slee287@gmu.edu.

1. Introduction

Large Gaussian and non-Gaussian spatial datasets with inherent spatial dependencies arise in numerous disciplines, including economics (Redding and Rossi-Hansberg, 2017), hydrology (Zhou and Li, 2020), public health (Rushton, 2003), and genetics (Wagner and Fortin, 2013). Advances in data collection technologies have enabled the acquisition of spatially indexed datasets comprising millions of observation locations, often over non-stationary and heterogeneous spatial domains.

To analyze such spatial data, a widely used approach is the spatial generalized linear mixed model (SGLMM) (Diggle, 1998). SGLMMs provide a flexible framework for modeling data with spatial random effects and have been extensively applied to both Gaussian and non-Gaussian spatially correlated datasets (Bonat and Ribeiro Jr, 2016; Lee and Park, 2023; Zilber and Katzfuss, 2021). The spatial random effects are typically modeled as latent Gaussian processes (GPs) with a specified spatial covariance function. Within a Bayesian hierarchical modeling framework (Wikle et al., 1998), posterior inference is commonly performed using Markov chain Monte Carlo (MCMC) methods. However, when the latent variables are high-dimensional and exhibit strong spatial dependence, the Markov chains tend to mix slowly (Haran et al., 2003), and the associated computational costs scale cubically with the number of locations.

Scalable approaches for spatial models have been developed including low-rank and basis representations (Cressie and Johannesson, 2008; Banerjee et al., 2008; Katzfuss, 2017; Higdon, 1998; Cressie, 2015) and methods that exploit sparsity in covariance or precision matrices, such as the nearest neighbor Gaussian process (NNGP) (Datta et al., 2016), Vecchia approximations (Katzfuss, 2017), and covariance tapering (Furrer et al., 2006). Other strategies include integrated nested Laplace approximations (INLA) (Rue et al., 2009), as well as conjugate spatial models such as Pólya–Gamma mixtures (Polson et al., 2013) and latent conjugate models (Bradley et al., 2020). While these approaches offer substantial computational gains, many still require MCMC-based posterior sampling, which becomes prohibitive for very large datasets, or depend on normality and Laplace approximations that are known to underestimate uncertainty (Ferklingstad and Rue, 2015).

Variational Bayes (VB) (Blei and Jordan, 2006; Fox and Roberts, 2012; Jordan et al., 1999) is an optimization approach that approximates the target distribution (e.g., posterior distribution) by specifying a variational distribu-

tion that minimizes the Kullback–Leibler (KL) divergence from the target. Variants such as mean-field variational Bayes (MFVB) (Mohammad-Djafari and Ayasso, 2009; Han and Yang, 2019; Blei and Jordan, 2006), hybrid MFVB methods (Wang and Blei, 2013; Tran et al., 2021), and integrated non-factorized variational Bayes (INFVB) (Han et al., 2013; Lee and Lee, 2024) have become popular among practitioners for analyzing large datasets efficiently. Semi-implicit variational inference (SIVI) (Yin and Zhou, 2018) defines the variational mixing distribution through a neural network; thereby providing the flexibility needed to adequately model dependence in multivariate posterior distributions.

However, the application of VB methods to continuous spatial domains for non-Gaussian SGLMMs remains limited. Ren et al. (2011) applied VB to small Gaussian spatial datasets. Wu (2018) use integrated non-factorized variational Bayes (INFVB) for Gaussian areal data, and Bansal et al. (2021) and Parker et al. (2022) modeled count and binary areal data. Cao et al. (2023) employed a variational approach with a sparse inverse Cholesky representation for the latent Gaussian process, achieving faster convergence compared to alternative methods. Lee and Lee (2024) propose a scalable INFVB approach for modeling non-Gaussian spatial data, but their approach is limited to spatial data from Gaussian, Bernoulli, and Poisson data distributions and relies on conjugate or near-conjugate approximations. Song and Datta (2025) embed NNGP within an MFVB framework; however, their approach applies only to Gaussian responses and inherits key limitations of MFVB, including block-independence assumptions and variational functions that can underestimate posterior variances (Blei and Jordan, 2006; Han et al., 2013). Garneau et al. (2025) incorporate NNGP within SIVI, but their framework is restricted to Gaussian and small Poisson datasets (e.g., $n = 500$) and does not cover other response types such as negative binomial, gamma, or Bernoulli. Moreover, their large-scale application focuses on Gaussian spatial data, where the latent spatial random effects are readily integrated out; thus, notably reducing the number of estimable model parameters.

We propose a scalable variational framework that integrates SIVI with spatial basis representations to enable fast Bayesian inference for large, continuous-domain SGLMMs across a range of non-Gaussian response types. By combining an implicit neural mixing distribution with an explicit Gaussian variational layer for the basis coefficients and fixed effects, our SIVI–basis approach flexibly captures posterior dependencies while remaining computationally efficient. The methodology accommodates a broad class of response

types, including negative binomial, gamma, Poisson, Bernoulli, and Gaussian, without relying on Laplace or conjugacy-based approximations. Through extensive simulation studies considering 20 scenarios and two real-world applications, we demonstrate that the proposed SIVI–basis framework achieves predictive accuracy and posterior summaries comparable to MCMC, while reducing computation time by an order of magnitude or more.

In the context of continuous-domain SGLMMs, there is a dearth of VB methods that simultaneously: (i) accommodates gamma and negative binomial responses with dispersion, alongside Bernoulli, Poisson, and Gaussian data; (ii) exploits basis representations to scale to large spatial datasets; and (iii) avoids ad hoc Laplace or quadratic approximations required for conditional conjugacy. Our proposed method fills this gap by adapting SIVI to SGLMMs in a way that preserves computational efficiency while enabling flexible inference for non-conjugate non-Gaussian spatial models.

The remainder of the paper is organized as follows. Section 2 provides an overview of SGLMMs and its basis representation extension (basis-SGLMM). In Section 3, we provide a review of variational Bayes and SIVI methods. We introduce our proposed SIVI-based inference framework for basis-SGLMMs and discusses algorithmic details in Section 4. Section 5 presents an extensive simulation study with comparisons to competing methods, and Section 6 applies the approach to two large non-Gaussian spatial datasets: one from remote sensing and one from the North American Breeding Bird Survey. Section 7 concludes with a discussion of limitations, practical guidance, and directions for future research.

2. Spatial Generalized Linear Mixed Models (SGLMMs)

Spatial generalized linear mixed models (SGLMMs) (Diggle, 1998) are a widely used framework for modeling non-Gaussian spatial data, supporting diverse response types (Bonat and Ribeiro Jr, 2016) and spatially-correlated random effects. Let $\mathbf{Z} = \{\mathbf{Z}(\mathbf{s}_i)\}_{i=1}^N$ denote the observations collected at spatial locations $\mathbf{s}_i \in \mathbf{S} \subseteq \mathbb{R}^2$, and let $\mathbf{X} \in \mathbb{R}^{N \times p}$ be the corresponding matrix of covariates. Spatial dependence is introduced via the random effects $\boldsymbol{\omega} = \{\boldsymbol{\omega}(\mathbf{s}_i)\}_{i=1}^N \in \mathbb{R}^N$, often modeled as a zero-mean Gaussian process with covariance function $C(\Psi)$, where Ψ represents the covariance parameters. For a finite set of locations, the spatial random effects follow a multivariate normal distribution $\boldsymbol{\omega} \sim \mathcal{N}(\mathbf{0}, \boldsymbol{\Sigma}(\Psi))$, with covariance matrix $\boldsymbol{\Sigma}(\Psi) \in \mathbb{R}^{N \times N}$ such that $\boldsymbol{\Sigma}(\Psi)_{ij} = C(\Psi)_{ij}$ for sites \mathbf{s}_i and \mathbf{s}_j . To simplify notation, we set

$Z_i := Z(\mathbf{s}_i)$, and $\omega_i := \omega(\mathbf{s}_i)$. The Bayesian hierarchical formulation of the SGLMM is

$$\begin{aligned} \text{Data model: } Z_i | \boldsymbol{\beta}, \boldsymbol{\omega}, \gamma &\stackrel{\text{ind}}{\sim} F(\cdot | \eta_i, \gamma), \quad i = 1, \dots, n, \\ &g\{\mathbb{E}(Z_i | \boldsymbol{\beta}, \omega_i)\} = \eta_i = \mathbf{x}(\mathbf{s}_i)^\top \boldsymbol{\beta} + \omega_i, \\ \text{Process model: } \boldsymbol{\omega} | \Psi &\sim \mathcal{N}_n(\mathbf{0}, \boldsymbol{\Sigma}(\Psi)), \\ \text{Parameter model: } \boldsymbol{\beta} &\sim p(\boldsymbol{\beta}), \quad \Psi \sim p(\Psi), \quad \gamma \sim p(\gamma) \end{aligned} \tag{1}$$

where $F(\cdot)$ denotes the probability distribution of the response (e.g., Normal for Gaussian data or Negative Binomial for count data), and $g(\cdot)$ is a known link function applied componentwise. $\boldsymbol{\beta} \in \mathbb{R}^p$ denotes the regression coefficients. $\mathbf{x}(\mathbf{s}_i)$ is the row of \mathbf{X} corresponding to the location \mathbf{s}_i . The additional parameter γ represents the extra distributional parameter corresponding to each response type; for example, the nugget variance τ^2 for the Gaussian model and the dispersion parameters α and κ for the Gamma and negative binomial models. In this study, we consider $\gamma \in \{\tau^2, \kappa, \alpha\}$. The prior distributions are $p(\boldsymbol{\beta})$, $p(\Psi)$, and $p(\gamma)$. If not stated otherwise, we assume a prior independence, so that $p(\boldsymbol{\beta}, \Psi, \gamma) = p(\boldsymbol{\beta}) p(\Psi) p(\gamma)$. In this study, we employ the logit link function for the Bernoulli case and the log link function for the Poisson, gamma, and negative binomial cases.

In practice, SGLMMs face substantial computational challenges when applied to large datasets. First, matrix operations involving dense $N \times N$ covariance matrices are prohibitive, as Cholesky decompositions require $\mathcal{O}(N^3)$ floating-point operations. Next, the spatial random effects $\{\omega_i\}_{i=1}^N$ are often strongly correlated, which can lead to poor mixing in Markov chain Monte Carlo (MCMC) algorithms (Haran et al., 2003). Finally, SGLMMs are overparameterized, requiring inference for the full set of latent spatial effects $\boldsymbol{\omega}_i$.

2.1. Basis Representations of SGLMMs (Basis-SGLMM)

To address computational issues associated with fitting SGLMMs to large datasets, basis representations of $\boldsymbol{\omega}$ (basis-SGLMM) (Higdon, 1998; Sengupta and Cressie, 2013; Bradley et al., 2016; Lee and Haran, 2022; Lee and Park, 2023) have been employed to reduce the dimensionality of $\boldsymbol{\omega}$, bypass costly operations on large matrices, and weaken the correlations across the spatial random effects $\boldsymbol{\omega}_i$.

In basis-SGLMMs, $\omega(\mathbf{s}_i)$ is represented as a basis expansion of m spatial

basis functions. Specifically, $\boldsymbol{\omega} \approx \boldsymbol{\Phi} \boldsymbol{\delta}$, where $\boldsymbol{\Phi} \in \mathbb{R}^{N \times m}$ is the matrix of basis functions where the j th column $\boldsymbol{\Phi}_j$ contains the j th basis function evaluated at all locations \mathbf{s}_i and $\boldsymbol{\delta} \in \mathbb{R}^m$ denotes the corresponding basis coefficients.

The Bayesian hierarchical model for the basis representation of SGLMMs is given by

$$\begin{aligned} \text{Data model: } Z_i | \boldsymbol{\beta}, \boldsymbol{\delta} &\stackrel{\text{ind}}{\sim} F(\cdot | \eta_i, \gamma), \quad i = 1, \dots, N, \\ g(\mathbb{E}[Z_i | \boldsymbol{\beta}, \boldsymbol{\delta}]) &= \eta_i = \mathbf{x}(\mathbf{s}_i)^\top \boldsymbol{\beta} + \boldsymbol{\Phi}(\mathbf{s}_i)^\top \boldsymbol{\delta}, \\ \text{Process model: } \boldsymbol{\delta} | \zeta &\sim \mathcal{N}_m(\mathbf{0}, \boldsymbol{\Sigma}_\delta(\zeta)), \\ \text{Parameter model: } \boldsymbol{\beta} &\sim p(\boldsymbol{\beta}), \quad \zeta \sim p(\zeta), \quad \gamma \sim p(\gamma) \end{aligned} \tag{2}$$

where $\boldsymbol{\Sigma}_\delta(\zeta)$ denotes the prior covariance matrix for the basis coefficients $\boldsymbol{\delta}$, with covariance parameters ζ . The prior distribution for ζ is $p(\zeta)$. $\boldsymbol{\Phi}(\mathbf{s}_i)$ denotes the row of $\boldsymbol{\Phi}$ corresponding to the location \mathbf{s}_i . We assume that the basis functions comprising $\boldsymbol{\Phi}$ are fixed prior to model fitting.

A key advantage of the basis representation is the substantial dimension reduction it affords, since $\boldsymbol{\delta} \in \mathbb{R}^m$ with $m \ll N$. This reduction not only lowers computational costs ($\mathcal{O}(nm)$) for fitting the model but also weakens the dependence among the components of $\boldsymbol{\delta}$, leading to faster-mixing Markov chains (Haran et al., 2003). MCMC algorithms can be prohibitive in large- N since each iteration of the algorithm becomes computationally expensive, often resulting in low effective samples per second and long walltimes. The low-dimensional parameter vector $(\boldsymbol{\beta}, \boldsymbol{\delta}, \sigma^2, \gamma)$ is the focus of our SIVI approximation in Section 4.

3. Variational Inference

Variational Bayes (VB) methods frame Bayesian inference as an optimization problem rather than relying on sampling-based approaches such as MCMC (Bishop, 2006). Let \mathbf{Z} denote the observed data, $\boldsymbol{\theta}$ the collection of latent variables and parameters, and $\boldsymbol{\psi}$ the variational parameters. VB approximates the target posterior $p(\boldsymbol{\theta} | \mathbf{Z})$ by introducing a variational distribution $q(\boldsymbol{\theta} | \boldsymbol{\psi})$ and choosing $\boldsymbol{\psi}$ to minimize the Kullback-Leibler (KL) divergence

$$q^*(\boldsymbol{\theta} | \boldsymbol{\psi}) = \arg \min_{q \in \mathcal{Q}} \text{KL}(q(\boldsymbol{\theta} | \boldsymbol{\psi}) \| p(\boldsymbol{\theta} | \mathbf{Z})),$$

where

$$\begin{aligned} \text{KL}(q(\boldsymbol{\theta} \mid \boldsymbol{\psi}) \parallel p(\boldsymbol{\theta} \mid \mathbf{Z})) &= \mathbb{E}_q \left[\log \frac{q(\boldsymbol{\theta} \mid \boldsymbol{\psi})}{p(\boldsymbol{\theta} \mid \mathbf{Z})} \right] \\ &= - \int q(\boldsymbol{\theta} \mid \boldsymbol{\psi}) \log \frac{p(\mathbf{Z} \mid \boldsymbol{\theta})p(\boldsymbol{\theta})}{q(\boldsymbol{\theta} \mid \boldsymbol{\psi})} d\boldsymbol{\theta} + \log p(\mathbf{Z}). \end{aligned} \quad (3)$$

Since the KL divergence is non-negative, minimizing $\text{KL}(q(\boldsymbol{\theta} \mid \boldsymbol{\psi}) \parallel p(\boldsymbol{\theta} \mid \mathbf{Z}))$ is equivalent to maximizing a lower bound on the marginal log-likelihood $\log p(\mathbf{Z})$, commonly referred to as the Evidence Lower Bound (ELBO) (Bishop and Tipping, 2013; Blei and Jordan, 2006):

$$\text{ELBO}(q) := \int q(\boldsymbol{\theta} \mid \boldsymbol{\psi}) \log \frac{p(\mathbf{Z} \mid \boldsymbol{\theta}) \cdot p(\boldsymbol{\theta})}{q(\boldsymbol{\theta} \mid \boldsymbol{\psi})} d\boldsymbol{\theta} = \mathbb{E}_q \left(\log \frac{p(\mathbf{Z} \mid \boldsymbol{\theta}) \cdot p(\boldsymbol{\theta})}{q(\boldsymbol{\theta} \mid \boldsymbol{\psi})} \right). \quad (4)$$

Coordinate Ascent and Implicit Variational Inference. An important design choice is the specification of the variational family \mathcal{Q} and constraints imposed on $q(\boldsymbol{\theta})$ (Tran et al., 2021). A common choice is the mean-field variational Bayes (MFVB) approximation, which factorizes the joint variational density as $q(\boldsymbol{\theta}) = \prod_{k=1}^K q_k(\boldsymbol{\theta}_k)$ where $\boldsymbol{\theta} = (\boldsymbol{\theta}_1, \dots, \boldsymbol{\theta}_K)$ denotes blocks of parameters and latent variables, and q_k is the variational density for block k . Under this factorization, the ELBO can be optimized by coordinate-ascent variational inference (CAVI), which updates each q_k in turn using closed-form expressions when conjugacy is available (Blei et al., 2017).

While CAVI is computationally efficient, it is well known to underestimate posterior and posterior predictive variances and may not fully capture dependence among parameters (Blei and Jordan, 2006; Han et al., 2013; Blei et al., 2017; Wu, 2018). Moreover, these methods have either relied on conditionally conjugate models (Wang and Blei, 2013). While MFVB can address some non-conjugate models via analytic approximations, such as Laplace approximations for counts or quadratic bounds for Bernoulli data (Jaakkola and Jordan, 1997; Lee and Lee, 2024), these approaches do not readily extend to more complex distributions like gamma or negative binomial responses.

Implicit variational families (Mohamed and Lakshminarayanan, 2016; Tran et al., 2017; Li and Turner, 2017; Shi et al., 2017; Huszár, 2017; Mescheder et al., 2017) have been proposed to increase flexibility and restore dependencies beyond mean-field factorizations by defining the variational distribution

$q_\lambda(\boldsymbol{\theta})$ only through a generative mechanism:

$$\boldsymbol{\theta} = g_\lambda(\boldsymbol{\epsilon}), \quad \boldsymbol{\epsilon} \sim p(\boldsymbol{\epsilon}), \quad (5)$$

where g_λ is a deterministic transformation parameterized by λ and $p(\boldsymbol{\epsilon})$ is a base distribution (e.g. Gaussian). Though flexible, the resulting $q_\lambda(\boldsymbol{\theta})$ is defined implicitly, meaning that sampling from it is straightforward, but the density is not available in closed form. The lack of an explicit density prevents direct evaluation of the log-density term $\log q_\lambda(\boldsymbol{\theta}) - \log p(\boldsymbol{\theta}, \mathbf{Z})$ in the ELBO in (4). In contrast, an explicit family provides a tractable density for every z .

3.1. Semi-implicit Variational Inference

Semi-implicit variational inference (SIVI) (Yin and Zhou, 2018) provides a compromise between explicit and fully implicit variational families. SIVI augments an explicit base variational distribution with an implicit mixing distribution to form a hierarchical variational model. Let $\boldsymbol{\psi}$ denote an auxiliary variable and ϕ the parameters of a mixing distribution $q_\phi(\boldsymbol{\psi})$. The semi-implicit variational family is defined hierarchically as

$$\boldsymbol{\theta} \sim q(\boldsymbol{\theta} \mid \boldsymbol{\psi}), \quad \boldsymbol{\psi} \sim q_\phi(\boldsymbol{\psi}), \quad (6)$$

where $q(\boldsymbol{\theta} \mid \boldsymbol{\psi})$ is an explicit, reparameterizable distribution (e.g., Gaussian) and $q_\phi(\boldsymbol{\psi})$ may be either explicit or implicit (e.g., represented by a neural network). Marginalizing over $\boldsymbol{\psi}$ yields the semi-implicit variational density

$$h_\phi(\boldsymbol{\theta}) = \int q(\boldsymbol{\theta} \mid \boldsymbol{\psi}) q_\phi(\boldsymbol{\psi}) d\boldsymbol{\psi} = \mathbb{E}_{\boldsymbol{\psi} \sim q_\phi(\boldsymbol{\psi})} [q(\boldsymbol{\theta} \mid \boldsymbol{\psi})]. \quad (7)$$

This construction restores dependencies among components of $\boldsymbol{\theta}$ while retaining the explicit conditional density $q(\boldsymbol{\theta} \mid \boldsymbol{\psi})$ required for ELBO-based optimization. Direct evaluation of $h_\phi(\boldsymbol{\theta})$ is generally intractable when $q_\phi(\boldsymbol{\psi})$ is implicit, but Yin and Zhou (2018) provide a tractable surrogate lower bound on the ELBO ($\underline{\mathcal{L}}$) that is asymptotically tight and depends only on $q(\boldsymbol{\theta} \mid \boldsymbol{\psi})$ and samples from $q_\phi(\boldsymbol{\psi})$:

$$\underline{\mathcal{L}} = \mathbb{E}_{\boldsymbol{\psi} \sim q_\phi(\boldsymbol{\psi})} \mathbb{E}_{\boldsymbol{\theta} \sim q(\boldsymbol{\theta} \mid \boldsymbol{\psi})} \left[\log \frac{p(\mathbf{Z}, \boldsymbol{\theta})}{q(\boldsymbol{\theta} \mid \boldsymbol{\psi})} \right].$$

Note that $\underline{\mathcal{L}}$ depends only on $q(\boldsymbol{\theta} \mid \boldsymbol{\psi})$ and incorporates $q_\phi(\boldsymbol{\psi})$ (i.e., the

implicit distribution) solely through Monte Carlo samples. Moreover, $\underline{\mathcal{L}}$ is asymptotically exact to the true ELBO (Yin and Zhou, 2018); thereby allowing SIVI to retain the flexibility of implicit variational families while making ELBO optimization tractable via Monte Carlo methods. (see supplement S.2 for details)

Reparameterization and Multilayer Perceptron. SIVI optimizes the ELBO using stochastic gradients (Hoffman et al., 2013), but the ELBO contains expectations whose gradients cannot be directly evaluated because $q(\boldsymbol{\theta} \mid \boldsymbol{\psi})$ depends on $\boldsymbol{\psi}$.

The reparameterization trick (Kucukelbir et al., 2017) addresses this by expressing samples from $q_{\boldsymbol{\psi}}$ as deterministic transformations of auxiliary noise variables $g_{\boldsymbol{\psi}}(\epsilon)$ where $\epsilon \sim p_0(\epsilon)$ for some distribution $p_0(\cdot)$. This allows gradients to pass through expectations:

$$\nabla_{\boldsymbol{\psi}} \mathbb{E}_{q_{\boldsymbol{\psi}}(g_{\boldsymbol{\psi}}(\epsilon))} [f(g_{\boldsymbol{\psi}}(\epsilon))] = \mathbb{E}_{\epsilon \sim p_0} [\nabla_{\boldsymbol{\psi}} f(g_{\boldsymbol{\psi}}(\epsilon))] .$$

This yields low-variance gradient estimators and enables the use of automatic differentiation for variational optimization.

In this study, samples of $\boldsymbol{\psi}$ are obtained by passing random noise ϵ through a neural network, which provides a reparameterized representation of $q_{\phi}(\boldsymbol{\psi})$. Specifically, we employ a Multi-Layer Perceptron (MLP) (Almeida, 2020; Popescu et al., 2009) with the output layer defined as $\hat{y} = f(\mathbf{W}X + \mathbf{B})$ where \hat{y} denotes the output layer, \mathbf{W} the weight matrix, X the input layer, \mathbf{B} the bias vector, and $f(\cdot)$ a nonlinear activation function (e.g., ReLU, sigmoid, or tanh). ϕ corresponds to the weights and biases of a MLP, which are updated at each iteration to increase the flexibility of the posterior approximation. When a deep neural network is used to represent $q_{\phi}(\boldsymbol{\psi})$, the resulting distribution is implicit and the transformation is generally non-invertible. Nevertheless, $q_{\phi}(\boldsymbol{\psi})$ can be highly expressive, allowing complex dependencies among parameters to be captured. Once ϕ is updated, the MLP generates samples of $\boldsymbol{\psi}$, which are then used to estimate both the latent variables and the observed data. Conceptually, this construction can be viewed hierarchically as $\epsilon \rightarrow \boldsymbol{\psi} \rightarrow \boldsymbol{\theta}$ where random noise ϵ is transformed into $\boldsymbol{\psi}$ through the MLP, and $\boldsymbol{\psi}$ in turn defines the variational distribution of $\boldsymbol{\theta}$. We provide an algorithmic summary and workflow overview of SIVI in the Supplement.

4. Semi-Implicit Variational Inference for Basis-SGLMMs

We integrate the SIVI into the basis-SGLMM framework to enable scalable analysis of large spatial datasets ($N \approx 50,000$) without MCMC. The proposed approach accommodates response types from a broad class of response distributions, including gamma, negative binomial, Poisson, Bernoulli, and Gaussian distributions. The Bayesian hierarchical formulation of the proposed model is:

$$\begin{aligned}
\text{Data model: } Z_i | \boldsymbol{\beta}, \boldsymbol{\delta}, \gamma &\stackrel{\text{ind}}{\sim} F(\cdot | \eta_i, \gamma), \quad i = 1, \dots, N, \\
g(\mathbb{E}[Z_i | \boldsymbol{\beta}, \boldsymbol{\delta}]) &= \eta_i = \mathbf{x}(\mathbf{s}_i)^\top \boldsymbol{\beta} + \boldsymbol{\Phi}(\mathbf{s}_i)^\top \boldsymbol{\delta}, \\
\text{Process model: } \boldsymbol{\delta} | \sigma^2 &\sim \mathcal{N}(0, \sigma^2 \boldsymbol{\Sigma}_\delta) \\
\text{Parameter model: } \boldsymbol{\beta} &\sim p(\boldsymbol{\beta}), \quad \log \sigma^2 \sim \mathcal{N}(\mu_\sigma, \tau_\sigma^2), \quad \gamma \sim p(\gamma)
\end{aligned} \tag{8}$$

where μ_σ and τ_σ^2 represent the prior mean and variance of the reparameterized σ^2 . Depending on the chosen data model, the additional parameter γ is defined as one of $\gamma \in \{\log \tau^2, \kappa, \log \alpha\}$, and we assign priors accordingly: (i) $\log \tau^2 \sim \mathcal{N}(\mu_\tau, \sigma_\tau^2)$ for the Gaussian model; (ii) $\kappa \sim \text{Gamma}(a_\kappa, b_\kappa)$ for the negative binomial model; and (iii) $\log \alpha \sim \mathcal{N}(\mu_\alpha, \sigma_\alpha^2)$ for the gamma model. The basis functions $\boldsymbol{\Phi}$ are precomputed prior to applying the SIVI algorithm. The estimable parameters include $\boldsymbol{\beta}$, $\boldsymbol{\delta}$, σ^2 , and the response distribution-specific parameters τ^2 , α , and κ . Note that the Bayesian hierarchical model above presents only the conditional distributions and priors of the spatial model itself, and the variational components required for SIVI, (namely the implicit mixing distribution and explicit conditional variational distribution), are not shown. Instead, they are introduced in the following subsection.

Variational Inference for Basis-SGLMMs. We now describe the variational inference framework, including the associated variational distributions, for basis-SGLMMs. The SIVI workflow integrates readily with the basis-SGLMM framework by treating all model parameters and latent variables as unified parameter vector $\boldsymbol{\theta} = (\boldsymbol{\beta}, \boldsymbol{\delta}, \log \sigma^2, \gamma)$. Algorithm 1 summarizes the steps, and Figure 1 illustrates the SIVI workflow within the basis-SGLMM framework.

At each iteration of the algorithm, random noise $\epsilon_j \sim q(\epsilon)$ is generated and mapped through the multi-layer perceptron T_ϕ where ϕ denotes the MLP

weights and biases to obtain an implicit mixing variable ψ_j (Steps 1-3). This mixing variable parameterizes the explicit conditional variational distribution $q(\boldsymbol{\theta}_j \mid \psi_j)$, which must be chosen so that the reparameterization trick can be applied. In the context of a basis-SGLMM, ψ_j determines the variational mean or covariance for the low-dimensional basis coefficients δ as well as the fixed effects β , enabling the variational family to adaptively capture posterior dependence across these parameters. Since the latent spatial process is approximated using the precomputed basis matrix Φ (with $\omega \approx \Phi\delta$), sampling $\boldsymbol{\theta}_j$ avoids the need to manipulate high-dimensional Gaussian process realizations; thereby substantially reducing computational cost.

To construct the semi-implicit variational density $h_\phi(\boldsymbol{\theta})$, SIVI draws an additional set of auxiliary noise variables $\epsilon^{(k)}$ and generates corresponding mixing variables $\psi^{(k)} = T_\phi(\epsilon^{(k)})$ (Steps 5-7). New samples of $\boldsymbol{\theta}$ are then drawn from $q(\boldsymbol{\theta}_j \mid \psi^{(k)})$ (Step 8), and the entire collection of samples is used to compute the surrogate lower bound of ELBO (\mathcal{L}) that approximates the marginal density $h_\phi(\boldsymbol{\theta})$ (Step 9). This ELBO (\mathcal{L}) incorporates the non-Gaussian likelihood of the basis-SGLMM as well as the spatial structure induced by the basis expansion. The algorithm iteratively updates the neural network parameters ϕ until the ELBO (\mathcal{L}) converges (Step 10), resulting in a flexible variational posterior that captures complex dependencies among $\boldsymbol{\theta} = (\boldsymbol{\beta}, \boldsymbol{\delta}, \log \sigma^2, \gamma)$ while remaining computationally scalable for large spatial datasets.

4.1. Implementation Details

The proposed SIVI algorithm requires the specification of several tuning parameters prior to implementation. These include the : (i) stopping criterion threshold ϵ_* ; (ii) maximum number of iterations for optimization; (iii) batches J used when generating samples; (iv) number of auxiliary samples K ; (v) scale parameters for the conditional (explicit) distribution; and (vi) choice of reparameterized priors used for gradient-based optimization.

First, the stopping criterion threshold ϵ_* must be specified. To examine the effect of different stopping criteria on SIVI performance, we conduct a sensitivity analysis using different stopping criteria (10^{-1} , 10^{-3} , and 10^{-4}) and compare metrics such as RMSPE and walltime across different methods. Using a smaller threshold (e.g., $\epsilon_* = 10^{-3}$ or 10^{-4}) increases walltime but yields only modest gains in predictive accuracy (see Section S.4.1). Larger thresholds reduce computational times but risk underestimating posterior uncertainty. In practice, the stopping criterion should be set by balancing

Algorithm 1 Semi-Implicit Variational Inference (SIVI) for Basis-SGLMMs

- 1: **Input:** Data $\{\mathbf{Z}_i\}_{1:N}$, likelihood $p(Z_i \mid \boldsymbol{\beta}, \boldsymbol{\delta}, \log \sigma^2, \gamma)$, basis matrix $\boldsymbol{\Phi}$, joint model $p(\mathbf{Z}, \boldsymbol{\theta})$ where $\boldsymbol{\theta} = (\boldsymbol{\beta}, \boldsymbol{\delta}, \log \sigma^2, \gamma)$, explicit variational distribution $q(\boldsymbol{\theta} \mid \boldsymbol{\psi})$ with reparameterization $\boldsymbol{\theta} = f(\epsilon, \boldsymbol{\psi})$, implicit MLP layer $T_\phi(\epsilon)$, and noise source $\epsilon \sim q(\epsilon)$
- 2: **Output:** Implicit variational parameter ϕ defining the mixing distribution $q_\phi(\boldsymbol{\psi})$

3: Initialize ϕ randomly

4: **while** not converged **do**

5: Set $\underline{L}_{K_t} = 0$ and step size η_t ; choose non-decreasing $K_t \geq 0$

6: Sample variables $\boldsymbol{\psi}^{(k)} = T_\phi(\epsilon^{(k)})$ with $\epsilon^{(k)} \sim q(\epsilon)$ for $k = 1, \dots, K_t$

7: **for** $j = 1$ to J **do**

8: Sample $\boldsymbol{\psi}_j = T_\phi(\epsilon_j)$ with $\epsilon_j \sim q(\epsilon)$

9: Sample $\boldsymbol{\theta}_j = f(\tilde{\epsilon}_j, \boldsymbol{\psi}_j)$, $\boldsymbol{\theta}_j = (\boldsymbol{\beta}_j, \boldsymbol{\delta}_j, \log \sigma_j^2, \gamma_j)$ and $\tilde{\epsilon}_j \sim p(\epsilon)$

10:

11: Compute contribution to the surrogate lower bound of ELBO ($\underline{\mathcal{L}}$):

$$\underline{L}_{K_t} \leftarrow \underline{L}_{K_t} + \frac{1}{J} \left\{ -\log \frac{1}{K_t + 1} \left[\sum_{k=1}^{K_t} q(\boldsymbol{\theta}_j \mid \boldsymbol{\psi}^{(k)}) + q(\boldsymbol{\theta}_j \mid \boldsymbol{\psi}_j) \right] + \log p(\mathbf{Z} \mid \boldsymbol{\theta}_j) + \log p(\boldsymbol{\theta}_j) \right\}$$

12: **end for**

13: $t \leftarrow t + 1$

14: Update implicit variational parameters ϕ (MLP weights and biases):

$$\phi \leftarrow \phi + \eta_t \nabla_\phi \underline{L}_{K_t} \left(\{\boldsymbol{\psi}^{(k)}\}_{1:K_t}, \{\boldsymbol{\psi}_j\}_{1:J}, \{\boldsymbol{\theta}_j\}_{1:J} \right)$$

15: **end while**

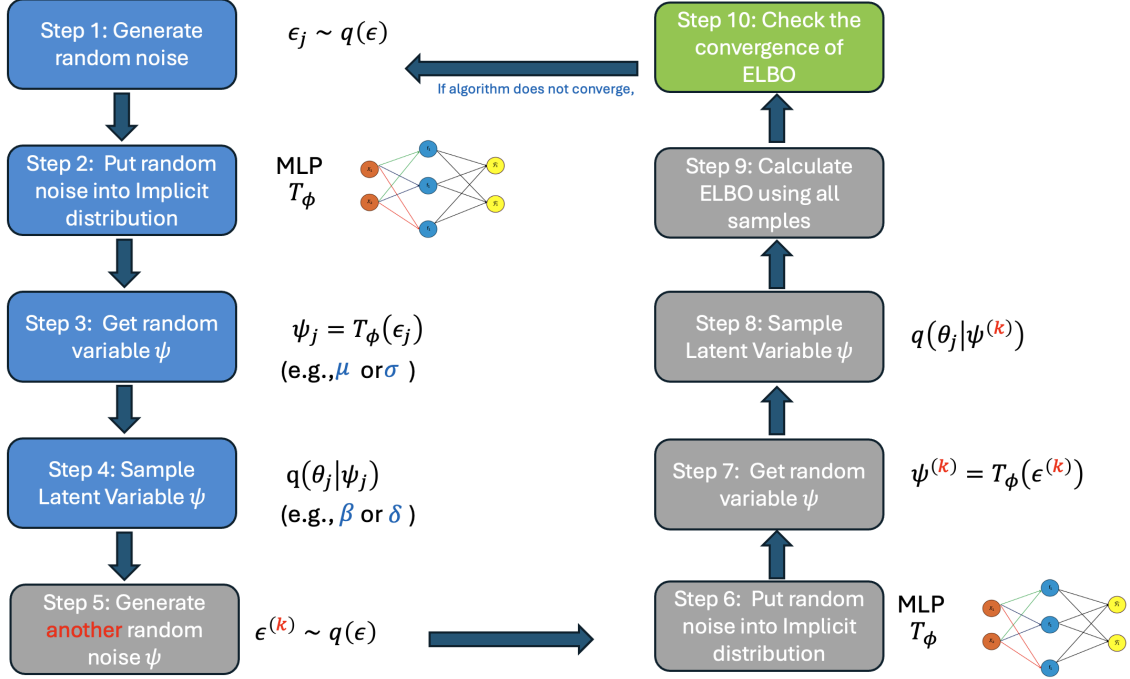


Figure 1: This illustrates an overview of the SIVI workflow of Algorithm 1

walltime against the desired predictive accuracy (e.g., RMSPE or AUC). In our simulation study (Section 5), we set the threshold to $\epsilon_* = 1 \times 10^{-2}$ (see Algorithm 1).

Second, the maximum number of optimization iterations must be specified; we set this to 5,000. Although a larger limit increases walltime, 5,000 iterations were sufficient in our experiments, with the loss function (negative ELBO) typically converging well before reaching this cap.

In Algorithm 1, K is the number of auxiliary samples used to approximate the mixing distribution. Using larger K results in a tighter surrogate ELBO but at higher computational costs. The parameter J denotes the number of Monte Carlo samples of θ used to estimate the surrogate ELBO and its gradient; larger J reduces variance but increases runtime. In our simulations, we set $J = 20$ and $K = 1,000$. Increasing either parameter can improve accuracy, but this comes at the cost of additional computation.

Fourth, the conditional explicit distribution is specified as

$$q_\phi(\boldsymbol{\theta} \mid \psi) = \mathcal{N}(\boldsymbol{\theta}; \mu_\phi(\psi), \text{diag}(\sigma^2)),$$

where $\mu_\phi(\psi)$ denotes the neural network output given the auxiliary noise ψ . Specifically, $\sigma_\beta, \sigma_\delta, \sigma_{\log \sigma^2}, \sigma_\alpha$ represent the fixed scale parameters (standard deviations) corresponding to the $\beta, \delta, \log \sigma^2$, and $\log \alpha$ coordinates, respectively. These scale parameters control the amount of smoothing in the SIVI family. Larger scales produce smoother and more stable gradient estimates but reduce flexibility. Smaller scales increase flexibility but raise gradient variance and may introduce instability in optimization. Although fixed in our implementation, learning these scales is a possible extension, albeit with additional computational costs.

Fifth, the explicit conditional distribution $q(\boldsymbol{\theta} \mid \boldsymbol{\psi})$ must either be reparameterizable or have a tractable analytic density. In contrast, the implicit mixing distribution $q_\phi(\boldsymbol{\psi})$ is required to be reparameterizable (through a noise transformation $\boldsymbol{\psi} = T_\phi(\epsilon)$), since its density is intractable (Yin and Zhou, 2018). Consequently, the choice of variational distributions is restricted to those that admit a reparameterization, which ensures the feasibility of gradient-based optimization within the SIVI framework.

5. Simulation Study

The proposed SIVI framework is evaluated through an extensive simulation study based on large spatial datasets ($N = 50,000$) generated under robust specifications, including varying response distributions, smoothness levels of the latent spatial random field, and decay in spatial correlation. Comparative analyses are conducted against competing approaches, including the Metropolis–Hastings (MH) algorithm and Hamiltonian Monte Carlo (HMC).

5.1. Simulation Design

We consider $N = 50,000$ spatial locations $\mathbf{s}_i \in \mathcal{D} = [0, 1]^2 \subset \mathbb{R}^2$, of which $N_{\text{train}} = 40,000$ are used for model fitting and $N_{\text{test}} = 10,000$ are reserved for validation. The observation vector $\mathbf{Z} = (Z(\mathbf{s}_1), \dots, Z(\mathbf{s}_N))^\top$ is generated under the basis-SGLMM framework described in subsection 2.1, with covariates $\mathbf{X} = [\mathbf{X}_1, \mathbf{X}_2]$ where $\mathbf{X}_1, \mathbf{X}_2 \stackrel{\text{i.i.d.}}{\sim} \text{Unif}(-1, 1)$ and regression coefficients $\boldsymbol{\beta} = (1, 1)^\top$. Four configurations of the spatial random effects

$\boldsymbol{\omega} = \{\omega(\mathbf{s}_i) : \mathbf{s}_i \in \mathcal{D}\}$ are generated from a zero-mean Gaussian process with a Matérn covariance function with covariance parameters ν , ϕ , and σ^2 .

Table S.1 summarizes the simulation design, which considers two smoothness parameters ($\nu \in 0.5, 1.5$) and two range parameters ($\phi \in 0.1, 0.3$) across five data types: Gamma, negative binomial, binary, count, and Gaussian. The marginal variance is fixed at $\sigma^2 = 1$. This yields 20 simulation scenarios, with 50 replicates per scenario, resulting in 1,000 datasets in total.

The basis-SGLMM approach (Section 2.1) is employed, approximating $\boldsymbol{\omega} \approx \boldsymbol{\Phi}\boldsymbol{\delta}$, where $\boldsymbol{\Phi}$ is an $n \times m$ matrix of spatial eigenbasis functions (Banerjee et al., 2008; Guan and Haran, 2018), taken as the m leading eigenvectors of a Matérn covariance matrix. Throughout, we use $m = 50$ basis functions. Priors are specified as $\boldsymbol{\beta}_j \sim \mathcal{N}(0, 100)$, $\log \tau^2 \sim \mathcal{N}(0, 1)$, $\log \sigma^2 \sim \mathcal{N}(1, 1)$, $\boldsymbol{\theta} \sim \text{Gamma}(2, 1)$, and $\log \alpha \sim \mathcal{N}(1, 1)$.

For SIVI, the stopping criterion is set to a threshold of $\epsilon_* = 1 \times 10^{-2}$ (see Algorithm 1). The maximum number of iterations is fixed at 5,000, and we set $J = 20$ as the number of samples per batch for SIVI. In this study, we utilize a multilayer perceptron (MLP) architecture consisting of three hidden layers of sizes 40, 60, and 40, respectively. Each pair of consecutive layers is fully connected, with the tanh function applied as the activation for the hidden layers and the linear activation function for the output layer. In our implementation of the MLP, we set the learning rate to 0.001 and Adam Algorithm (Kingma and Ba, 2014). For the MH algorithm, we obtain 100,000 posterior samples, assessing convergence via batch means standard errors (BMSE) (Flegal et al., 2008) and trace plots. For HMC, 2,000 posterior samples are drawn, which yield an effective sample size (ESS) (Liu and Liu, 2001) comparable to that of the MH sampler.

Model performance is evaluated using the root mean squared prediction error,

$$\text{RMSPE} = \sqrt{\frac{1}{N_{\text{test}}} \sum_{i=1}^{N_{\text{test}}} (Z_i - \hat{Z}_i)^2},$$

for the negative Binomial, gamma, count, and Gaussian data settings, and the area under the receiver operating characteristic curve (AUC) for the binary case.

All simulations are executed on a high-performance computing (HPC) system, with walltimes reported based on a single 2.4 GHz Intel Xeon Gold 6240R processor. The Metropolis–Hastings (MH) MCMC algorithm is im-

plemented in R version 4.1.2, while Hamiltonian Monte Carlo (HMC) and Semi-Implicit Variational Inference (SIVI) are implemented in PyTorch using Python (version 3.10.1).

5.2. Results

Results for inference and out-of-sample predictions are provided for the negative binomial and gamma cases. The Bernoulli, Poisson and Gaussian cases are available in the Supplement.

Negative Binomial Responses. Table 1 summarizes the out-of-sample predictive performance, measured by RMSPE, across all approaches. The results indicate that all three methods achieve nearly identical predictive accuracy. For instance, when the smoothness parameter is set to $\nu = 0.5$ and the spatial range parameter to $\phi = 0.1$, MH, HMC, and SIVI all yield an RMSPE of 3.473. However, the computational cost differs substantially: SIVI is approximately 44.4 times faster than MH and 2.0 times faster than HMC. Across the negative binomial experiments, the speedup of SIVI relative to MH ranges from 39 to 44, whereas the improvement relative to HMC is about a factor of two. Notably, the computational gains from SIVI would be even more pronounced under looser stopping criteria (see Supplements S.4.1, S.4.2, and S.4.3).

For all negative binomial datasets, the posterior distributions of the model parameters obtained from MH, HMC, and SIVI are largely comparable. Figure 2 illustrates this comparison for the regression coefficients (β_1, β_2) , variance components (σ^2, κ) , and selected spatial random effects (δ_5, δ_7) under the setting $\nu = 0.5$ and $\phi = 0.1$. Although variational methods are often noted for underestimating posterior variance (Blei and Jordan, 2006; Wu, 2018), our proposed SIVI approach not only achieves strong predictive accuracy but also produces posterior distributions that closely resemble those from MCMC-based methods, at least in our simulation study.

Table 1: Comparison of RMSPE, walltime (in seconds), and speedup for MH, HMC, and SIVI under different parameter settings for the negative binomial (NB) case.

	MH		HMC		SIVI		Speedup	
	RMSPE	Walltime	RMSPE	Walltime	RMSPE	Walltime	MH/SIVI	HMC/SIVI
NB, $\nu = 0.5$								
$\phi = 0.1$	3.473	3194.339	3.473	141.085	3.473	71.909	44.422	1.962
$\phi = 0.3$	3.930	3308.680	3.930	143.947	3.931	81.522	40.586	1.766
NB, $\nu = 1.5$								
$\phi = 0.1$	3.971	3162.185	3.971	126.351	3.971	79.344	39.854	1.592
$\phi = 0.3$	3.887	3334.172	3.887	151.783	3.888	78.383	42.537	1.936

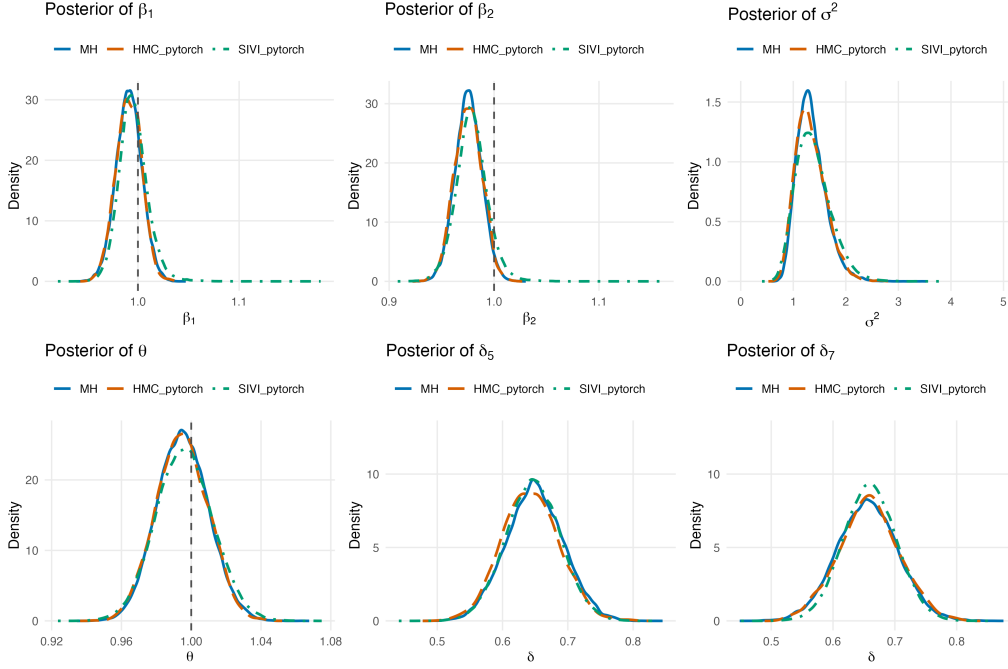


Figure 2: Posterior density estimates of selected model parameters under three inference methods for the negative binomial (NB) data when $\nu = 0.5$ and $\phi = 0.1$: Metropolis-Hastings (MH), Hamiltonian Monte Carlo (HMC), and Semi-Implicit Variational Inference (SIVI). Panels show results for regression coefficients (β_1, β_2), variance components (σ^2, κ), and selected spatial random effects (δ_5, δ_7). Dashed vertical lines indicate the corresponding true parameter values where available. Overall, all three methods yield nearly indistinguishable posterior distributions, highlighting the accuracy of SIVI relative to MCMC-based approaches.

Gamma Responses. Table 2 reports the RMSPE and walltime for Metropolis–Hastings (MH), Hamiltonian Monte Carlo (HMC), and Semi-Implicit Variational Inference (SIVI) applied to the gamma data using the 50 leading eigenvectors. Similar to the negative binomial results, all three methods achieve nearly identical predictive accuracy; however, the computational gains from SIVI are substantially greater. For example, when $\nu = 0.5$ and $\phi = 0.1$, MH, HMC, and SIVI all yield an RMSPE of 3.945, yet SIVI is approximately 145 times faster than MH and about 4 times faster than HMC. Across the gamma simulation studies, SIVI demonstrates speedups of 119–145 relative to MH and 3–4 relative to HMC. Notably, the gamma data provide the most pronounced computational advantage for SIVI compared with other models such as negative binomial, count, binary, and Gaussian.

As with the other data models, the posterior distributions of the model parameters obtained from MH, HMC, and SIVI remain largely consistent. Figure 3 illustrates this comparison for the setting $\nu = 0.5$ and $\phi = 0.3$.

Table 2: Comparison of RMSPE, walltime (in seconds), and speedup for MH, HMC, and SIVI under different parameter settings for the gamma case.

	MH		HMC		SIVI		Speedup	
	RMSPE	Walltime	RMSPE	Walltime	RMSPE	Walltime	MH/SIVI	HMC/SIVI
Gamma, $\nu = 0.5$								
$\phi = 0.1$	3.945	4291.942	3.945	121.865	3.945	29.560	145.193	4.123
$\phi = 0.3$	3.855	4071.220	3.855	129.565	3.855	32.061	126.985	4.041
Gamma, $\nu = 1.5$								
$\phi = 0.1$	4.614	4204.997	4.614	113.861	4.614	35.745	117.638	3.185
$\phi = 0.3$	3.559	4577.599	3.559	129.269	3.559	38.329	119.429	3.373

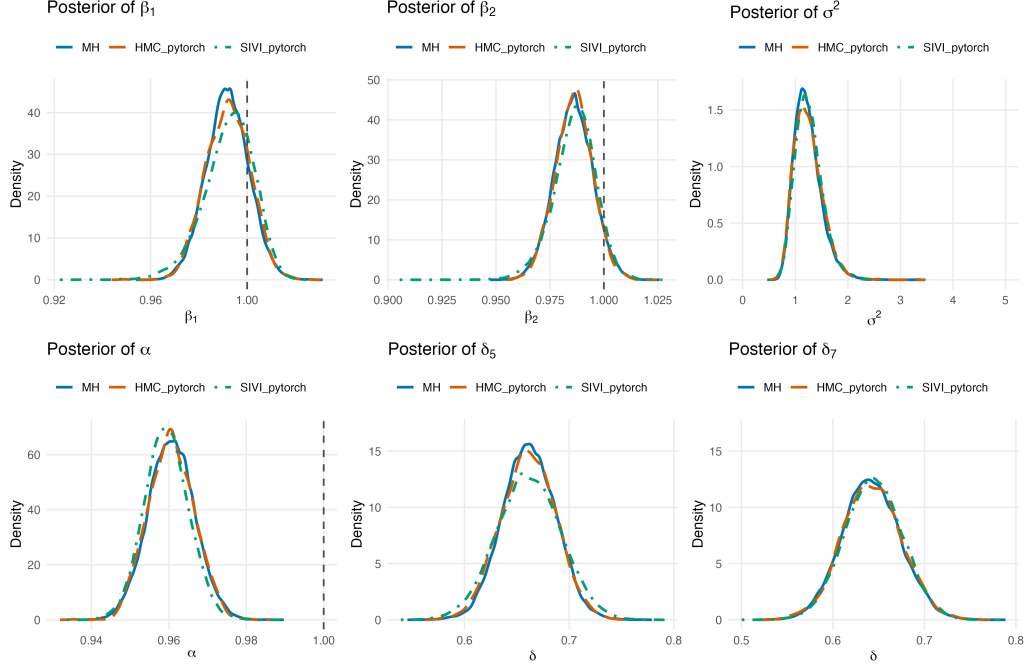


Figure 3: Posterior density estimates of selected model parameters under three inference methods for the gamma data $\nu = 0.5$ and $\phi = 0.3$: Metropolis-Hastings (MH), Hamiltonian Monte Carlo (HMC), and Semi-Implicit Variational Inference (SIVI). Panels show results for regression coefficients (β_1, β_2), variance components (σ^2, α), and selected spatial random effects (δ_5, δ_7). Dashed vertical lines indicate the corresponding true parameter values where available. Overall, all three methods yield nearly indistinguishable posterior distributions, highlighting the accuracy of SIVI relative to MCMC-based approaches.

5.2.1. Computational Costs

Table 3 summarizes the distribution of walltimes for MH, HMC, and SIVI across different data types, smoothness parameters, and spatial ranges. While the previous comparisons were based on mean walltimes, here we report the 25th, 50th (median), and 75th quantiles to capture the variability in computational costs. This quantile-based summary provides a more robust characterization, particularly since walltimes for SIVI methods can fluctuate across replications due to the seed of the samples and convergence behavior.

The results demonstrate that SIVI exhibits notable speedups across all data types and settings. For example, in the negative binomial and gamma

cases, SIVI reduces computation time by roughly 50 to 100 times compared to MH, and by factors of two to five relative to HMC. These speedup ratios are largely preserved across the 25th, 50th, and 75th percentiles. Binary and count data scenarios maintains speedups ranging from 20- to 70-fold relative to MH, and from 3- to 12-fold relative to HMC. Gaussian data show the smallest but still meaningful gains, with speedups of around 25- to 38-fold relative to MH and 2- to 4-fold relative to HMC. Based on these results, SIVI consistently delivers computational speedups over MCMC methods across data types and settings, even after accounting for variability in walltimes.

Table 3: Walltime quantiles (25%, 50%, 75%) for MH, HMC, and SIVI, and corresponding speedups (MH/SIVI, HMC/SIVI) across data types and smoothness settings.

	MH			HMC			SIVI			Speedup (MH/SIVI)			Speedup (HMC/SIVI)		
	25%	50%	75%	25%	50%	75%	25%	50%	75%	25%	50%	75%	25%	50%	75%
NB															
$\nu = 0.5$															
$\phi = 0.1$	3038.053	3205.406	3332.122	121.477	134.756	159.281	58.569	68.310	86.513	51.871	46.924	38.516	2.074	1.973	1.841
$\phi = 0.3$	3205.791	3337.000	3431.428	124.543	133.702	160.183	51.481	79.814	98.385	62.272	41.809	34.878	2.419	1.675	1.628
$\nu = 1.5$															
$\phi = 0.1$	3041.410	3165.704	3265.998	106.224	123.283	142.447	61.417	78.272	92.491	49.521	40.445	35.312	1.730	1.575	1.540
$\phi = 0.3$	3212.261	3385.727	3450.251	136.075	146.063	166.988	57.535	72.337	89.648	55.831	46.805	38.487	2.365	2.019	1.863
Gamma															
$\nu = 0.5$															
$\phi = 0.1$	3435.886	3540.562	3684.057	105.796	122.750	139.434	18.115	27.315	41.319	189.667	129.621	89.161	5.840	4.494	3.375
$\phi = 0.3$	3216.671	3337.640	3478.441	110.334	121.261	147.809	18.892	33.153	37.471	170.267	100.675	73.430	5.837	3.959	3.120
$\nu = 1.5$															
$\phi = 0.1$	3287.160	3479.287	3607.622	93.948	109.456	129.891	22.993	36.281	44.389	142.963	95.899	81.272	4.086	3.017	2.926
$\phi = 0.3$	2975.072	3150.037	3357.022	112.922	131.158	144.769	27.034	34.083	50.282	110.049	92.424	66.764	4.177	3.848	2.879
Binary															
$\nu = 0.5$															
$\phi = 0.1$	1102.228	1361.181	1534.596	178.892	184.339	195.206	14.728	22.249	29.604	74.840	61.180	51.837	12.147	8.285	6.594
$\phi = 0.3$	1100.464	1371.999	1527.190	179.067	184.389	191.079	17.481	26.021	33.474	62.952	52.727	45.623	12.743	7.086	5.708
$\nu = 1.5$															
$\phi = 0.1$	1060.812	1158.577	1504.216	176.950	179.799	184.318	15.382	27.420	31.645	68.962	42.253	47.535	11.503	6.557	5.825
$\phi = 0.3$	1048.858	1260.038	1503.935	179.101	182.640	189.276	18.710	26.934	34.497	56.058	46.782	43.596	9.572	6.781	5.487
Count															
$\nu = 0.5$															
$\phi = 0.1$	1043.119	1199.590	1228.619	183.496	200.628	216.618	39.466	50.036	50.036	26.431	23.975	24.555	4.649	4.010	4.329
$\phi = 0.3$	1045.639	1185.762	1239.167	169.726	184.288	201.212	42.037	54.113	69.422	24.874	21.913	17.850	4.038	3.406	2.889
$\nu = 1.5$															
$\phi = 0.1$	1089.074	1367.412	1515.595	158.783	182.745	202.656	41.847	56.343	63.753	26.025	24.270	23.773	3.794	3.243	3.179
$\phi = 0.3$	1100.422	1461.657	1525.157	157.560	182.322	205.267	46.807	57.893	65.707	23.510	25.247	23.211	3.366	3.149	3.147
Gaussian															
$\nu = 0.5$															
$\phi = 0.1$	560.900	678.775	692.222	53.365	60.349	72.330	18.163	23.028	27.417	30.873	29.476	25.248	2.937	2.621	2.638
$\phi = 0.3$	559.832	679.687	691.575	61.721	70.991	72.021	17.262	23.061	27.748	32.241	25.210	24.893	3.576	3.079	2.596
$\nu = 1.5$															
$\phi = 0.1$	672.899	681.511	688.272	57.222	67.887	79.427	17.947	27.621	31.509	37.494	24.654	21.848	3.188	2.456	2.524
$\phi = 0.3$	645.736	681.685	688.288	66.607	77.875	85.513	17.174	20.956	30.334	37.600	32.529	22.690	3.878	3.759	2.819

6. Applications

The proposed Semi-Implicit Variational Inference (SIVI) method is demonstrated using two real-world spatial datasets: (i) land surface temperature from the NASA Terra satellite (Zilber and Katzfuss, 2021), and (ii) Blue Jay bird-count data (Ziolkowski Jr., David et al., 2022). For benchmarking, we also compare SIVI with MH and HMC as in the simulation study.

6.1. MODIS Land Surface Temperature Data

NASA’s Terra Satellite Mission, part of the Earth Observing System Morning Constellation (EOS-AM), was launched on December 18, 1999, and began routine data acquisition in February 2000, providing continuous global observations of the Earth’s atmosphere, oceans, and cryosphere. We analyze land surface temperature (LST) obtained from NASA’s Moderate Resolution Imaging Spectroradiometer (MODIS) aboard the Terra satellite. LST data is contained in the MYD11_L2 product acquired on July 1, 2025, at 1:00 PM local time. The study region spans longitudes 16.5°–24.0° E and latitudes 36.0°–41.0° N, comprising 215,941 grid cells at a 1 km spatial resolution. For this demonstration, we randomly selected $n = 50,000$ locations for model fitting, reserving an additional 20% of the locations for validation.

Given that LST, in $^{\circ}C$, is strictly positive, the data are modeled using a basis-SGLMM with gamma-distributed responses and a log link function. The corresponding Bayesian hierarchical model within the SIVI framework is as follows :

$$\begin{aligned}
 \text{Data Model:} \quad & \mathbf{Z}|\boldsymbol{\beta}, \boldsymbol{\delta}, \alpha \sim \text{Gamma}(\boldsymbol{\alpha}, \boldsymbol{\alpha}e^{-\boldsymbol{\mu}}) \\
 & \text{where } \boldsymbol{\mu} = \exp(\mathbf{X}\boldsymbol{\beta} + \boldsymbol{\Phi}\boldsymbol{\delta}) \\
 \text{Process Model:} \quad & \boldsymbol{\delta}|\sigma^2 \sim \mathcal{N}(0, \sigma^2\boldsymbol{\Sigma}_{\delta}) \\
 \text{Parameter Model:} \quad & \boldsymbol{\beta} \sim \mathcal{N}(\boldsymbol{\mu}_{\beta}, \boldsymbol{\Sigma}_{\beta}), \\
 & \log \sigma^2 \sim \mathcal{N}(\mu_{\sigma}, \sigma_{\sigma}^2), \\
 & \log \alpha \sim \mathcal{N}(\mu_{\alpha}, \sigma_{\alpha}^2),
 \end{aligned}$$

where μ is the conditional mean, α denotes the shape parameter, \mathbf{X} is the matrix of covariates, $\boldsymbol{\beta}$ the regression coefficient vector, $\boldsymbol{\Phi}$ the basis function matrix, and $\boldsymbol{\delta}$ are the basis coefficients. The matrix $\boldsymbol{\Sigma}_{\delta}$ characterizes the spatial covariance structure, thereby inducing correlation across spatial

locations and capturing spatial dependence in the data. We represent the latent process using discretized Moran’s basis functions following Lee and Haran (2022). Specifically, the leading 100 eigenvectors were selected, as internal sensitivity checks indicated this choice balances number provided a balance between computational efficiency and predictive accuracy. The prior distributions were specified as $\beta \sim \mathcal{N}(0, 10^2)$, $\log \sigma^2 \sim \mathcal{N}(-8.84, 1.1)$, $\log \alpha \sim \mathcal{N}(1.270, 4.934)$, and $\delta \sim \mathcal{N}(0, \sigma^2 I)$. MH sampler is run for 100,000 iterations, while Hamiltonian Monte Carlo (HMC) is run for 2,000 iterations, which is consistent with the simulation experiments. We use $\epsilon_* = 1 \times 10^{-3}$ as the stopping criteria for SIVI.

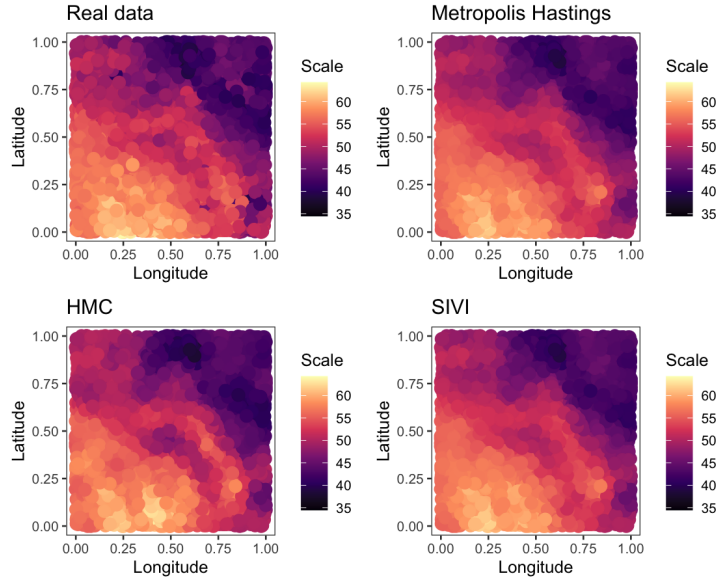


Figure 4: Interpolation results from modeling the MODIS land surface temperature data. Implementations of Metropolis–Hastings (MH) MCMC, Hamiltonian Monte Carlo (HMC), and Semi-Implicit Variational Inference (SIVI) with basis function representations are shown.

Though MH achieved the lowest RMSPE (1.42) but required 45 minutes (2,741 seconds) in Table 4 (a). In contrast, SIVI achieved a comparable RMSPE in only 262 seconds, representing a 10.46-fold speedup, while HMC attained a higher RMSPE of 1.85 with a runtime of 3.6 hours (12,826.73 seconds); thus making it 48.95 times slower than SIVI. Overall, these results

demonstrate that SIVI provides predictive accuracy comparable to MH and HMC while being approximately 10–to-49 times faster. Figure 4 illustrates the land surface temperature results, showing that all three methods produce visually similar outputs that effectively capture the hottest regions.

6.2. North American Breeding Bird Survey: Blue Jay Abundance

Jointly administered by the U.S. Geological Survey’s Eastern Ecological Science Center and the Canadian Wildlife Service of Environment Canada, the North American Breeding Bird Survey (BBS) (Ziolkowski Jr., David et al., 2022) is a long-term monitoring program that provides annual data on population trends and abundance for over 400 bird species across North America. We analyze observations of the Blue Jay (*Cyanocitta cristata*) collected in 2018 across 1,593 roadside survey sites (Figure 5). A total of 1,000 sites were used for model training, and the remaining 593 sites were held out for validation.

The analysis is conducted using the basis-SGLMM framework with a negative binomial response and the canonical log link function with the following hierarchical model:

$$\begin{aligned}
\text{Data Model:} \quad & \mathbf{Z} | \boldsymbol{\beta}, \boldsymbol{\delta}, \theta \sim \text{NB}(\boldsymbol{\mu}, \theta) \\
& \text{where } \boldsymbol{\mu} = \exp(\mathbf{X}\boldsymbol{\beta} + \boldsymbol{\Phi}\boldsymbol{\delta}) \\
\text{Process Model:} \quad & \boldsymbol{\delta} | \sigma^2 \sim \mathcal{N}(0, \sigma^2 \boldsymbol{\Sigma}_{\delta}) \\
\text{Parameter Model:} \quad & \boldsymbol{\beta} \sim \mathcal{N}(\boldsymbol{\mu}_{\beta}, \boldsymbol{\Sigma}_{\beta}), \\
& \log \sigma^2 \sim \mathcal{N}(\mu_{\sigma}, \sigma_{\sigma}^2) \\
& \theta \sim \text{Gamma}(a, b),
\end{aligned}$$

where $\boldsymbol{\beta}$ and $\boldsymbol{\delta}$ are the vectors of fixed-effect and basis coefficients, respectively. σ^2 denotes the prior marginal variance of $\boldsymbol{\delta}$, θ is the dispersion parameter, and \mathbf{X} is the design matrix containing geographic coordinates (latitude and longitude) and an intercept term. The basis function matrix $\boldsymbol{\Phi}$ is constructed from the leading 10 eigenvectors of a positive-definite covariance matrix defined using a Matérn covariance function with smoothness parameter $\nu = 0.5$ and range $\phi = 0.5$, evaluated at all sampled locations. Prior distributions are specified as $\boldsymbol{\beta} \sim \mathcal{N}([0, 0]', 100\mathbf{I}_2)$, $\log \sigma^2 \sim \mathcal{N}(1, 1)$, and $\theta \sim \text{Gamma}(2, 1)$. We compare the scalable SIVI approach with MH and HMC using the same implementation settings as the LST case.

The SIVI approach yields predictive accuracy on par with the MCMC-based approaches, while achieving substantially lower runtimes compared to both MH and HMC. Specifically, the SIVI implementation requires 13.968 seconds, corresponding to a computational speedup of 7.837 and 16.169 relative to MH and HMC, respectively in Table 4 (b). Although all three methods produce similar estimates of the latent intensity surface for Blue Jay abundance, as shown in Figure 5, SIVI achieves these results with considerably lower computational costs.

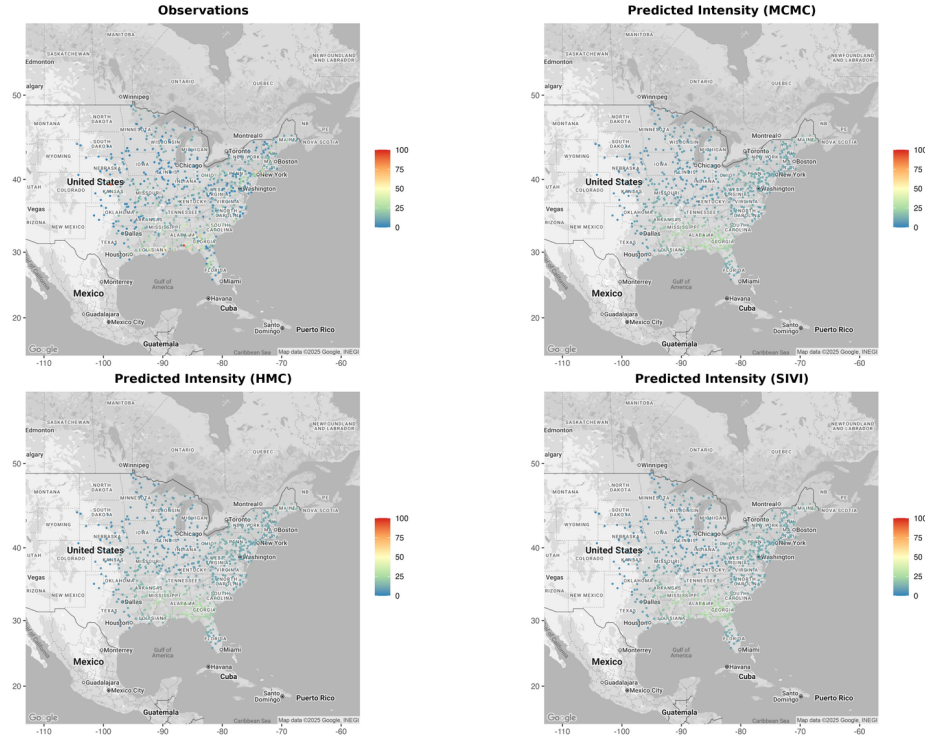


Figure 5: True observations (top-left) and predicted intensity surfaces for the North American Blue Jay abundance dataset. The intensity surface is estimated using the basis-SGLMM model fit via Metropolis Hastings MCMC (top-right), Hamiltonian Monte Carlo (HMC) (bottom-left), and Semi-Implicit Variational Inference (SIVI) (bottom-right).

Table 4: Predictive performance, computational cost, and speedup comparisons for the MODIS LST (50k locations) and Blue Jay abundance applications under Metropolis-Hastings (MH) MCMC, Hamiltonian Monte Carlo (HMC), and Semi-Implicit Variational Inference (SIVI). Wall times are reported in seconds, and computational speedup is defined as (MCMC walltime)/(SIVI walltime).

(a) MODIS Land Surface Temperature (LST)			
	MH MCMC	HMC	SIVI
RMSPE	1.42	1.85	1.43
Walltime (sec)	(2741.00)	(12826.73)	(262.05)
Computational Speedup	10.46	48.95	—

(b) Blue Jay abundance data			
	MH MCMC	HMC	SIVI
RMSPE	9.848	9.846	9.857
Walltime (sec)	(109.483)	(225.849)	(13.968)
Computational Speedup	7.837	16.169	—

7. Discussion

We develop an SIVI approach for modeling a wide range of spatially-correlated data types in the continuous spatial domain, including negative binomial, gamma, binary, count, and Gaussian. By integrating SIVI with basis-SGLMMs, our framework extends the applicability of spatial generalized linear mixed models to large-scale settings with spatial random effects, accommodating datasets of size $N = 50,000$. To the best of our knowledge, this is the first variational framework for continuous-domain non-Gaussian spatial data that accommodates gamma and negative binomial responses, alongside Bernoulli, Poisson, and Gaussian data, within a scalable basis-SGLMM setting. Existing VB methods have largely relied on conjugacy or strong approximations; by combining SIVI with basis-SGLMMs, we enable scalable inference without such restrictions. Through extensive simulation studies, we demonstrate that SIVI achieves results comparable to MCMC-based methods while delivering substantial computational advantages, with speedups ranging from 2-fold to 145-fold. More importantly, in our simu-

lation settings, the SIVI approach does not severely underestimate posterior variance, which is a common limitation of VB methods. We apply our method to land surface temperature and Blue Jay count data, achieving similar computational gains while preserving predictive accuracy and posterior uncertainty. These results demonstrate that SIVI enables scalable inference for large, non-Gaussian spatial datasets where traditional methods are impractical.

For the proposed approach, both the explicit conditional distribution $q(\boldsymbol{\theta} \mid \boldsymbol{\psi})$ and the implicit mixing distribution $q_\phi(\boldsymbol{\psi})$ must be from reparameterizable families, which limits modeling flexibility (Yin and Zhou, 2018). Particle SIVI (Lim and Johansen, 2024) relaxes this requirement for the mixing distribution, but the explicit conditional distribution must still be reparameterizable. More flexible, non-reparameterization-based approaches, such as Normalizing Flows (Rezende and Mohamed, 2015), Boosting Variational Inference (Guo et al., 2016), and Operator Variational Inference (Ranganath et al., 2016), could provide alternative variational distributions, particularly for more complex models (e.g., spatial extremes or spatio-temporal). Partitioned models (Lee and Park, 2023) may also improve posterior inference by fitting locally non-stationary models to the spatial domain. In addition, SIVI currently requires fixing scale parameters for the explicit variational distribution, and selecting these hyperparameters becomes increasingly difficult in high-dimensional settings. Allowing these scales to be learned automatically may improve model flexibility but would increase computational costs and introduce additional issues related to model convergence.

Extending SIVI to support subsampling could therefore enable inference on substantially larger spatial domains. Further opportunities include adapting the method to spatio-temporal and multivariate spatial processes (Wikle et al., 2019; Hamelijnck et al., 2021; Gneiting et al., 2010; Yarger et al., 2023), where computational demands remain a major bottleneck. While we focused on eigenvector and bisquare basis functions, many other basis representations, such as wavelets (Nychka et al., 2002) and empirical orthogonal functions (Cressie, 2015), could be readily embedded into the SIVI basis-SGLMM framework. Subsampling the datasets could help mitigate the computational complexity of evaluating the Evidence Lower Bound (ELBO). Moreover, subsampling naturally introduces gradient noise, which can act as a form of regularization by reducing the risk of overfitting and potentially improving convergence (Hoffman et al., 2013; Ranganath et al., 2013, 2014).

Data availability statement

The authors confirm that the data supporting the findings of this study are available within the article and its supplementary materials.

Funding

This research was not supported by any grants or funding.

Disclosure statement

No potential conflict of interest was reported by the authors.

References

- Almeida, L.B., 2020. Multilayer perceptrons, in: Handbook of neural computation. CRC Press, pp. C1–2.
- Banerjee, S., Gelfand, A.E., Finley, A.O., Sang, H., 2008. Gaussian predictive process models for large spatial data sets. *Journal of the Royal Statistical Society Series B: Statistical Methodology* 70, 825–848.
- Bansal, P., Krueger, R., Graham, D.J., 2021. Fast bayesian estimation of spatial count data models. *Computational Statistics & Data Analysis* 157, 107152.
- Bishop, C.M., 2006. *Pattern Recognition and Machine Learning (Information Science and Statistics)*. Springer-Verlag, Berlin, Heidelberg.
- Bishop, C.M., Tipping, M., 2013. Variational relevance vector machines. arXiv preprint arXiv:1301.3838 .
- Blei, D.M., Jordan, M.I., 2006. Variational inference for Dirichlet process mixtures. *Bayesian Analysis* 1, 121 – 143. URL: <https://doi.org/10.1214/06-BA104>, doi:10.1214/06-BA104.
- Blei, D.M., Kucukelbir, A., McAuliffe, J.D., 2017. Variational inference: A review for statisticians. *Journal of the American statistical Association* 112, 859–877.

- Bonat, W.H., Ribeiro Jr, P.J., 2016. Practical likelihood analysis for spatial generalized linear mixed models. *Environmetrics* 27, 83–89.
- Bradley, J.R., Cressie, N., Shi, T., 2016. A comparison of spatial predictors when datasets could be very large. *Statistics Surveys* 10, 100 – 131. URL: <https://doi.org/10.1214/16-SS115>, doi:10.1214/16-SS115.
- Bradley, J.R., Holan, S.H., Wikle, C.K., 2020. Bayesian hierarchical models with conjugate full-conditional distributions for dependent data from the natural exponential family. *Journal of the American Statistical Association* 115, 2037–2052.
- Cao, J., Kang, M., Jimenez, F., Sang, H., Schaefer, F.T., Katzfuss, M., 2023. Variational sparse inverse cholesky approximation for latent gaussian processes via double kullback-leibler minimization, in: *International Conference on Machine Learning*, PMLR. pp. 3559–3576.
- Cover, T.M., 1999. *Elements of information theory*. John Wiley & Sons.
- Cressie, N., 2015. *Statistics for spatial data*. John Wiley & Sons.
- Cressie, N., Johannesson, G., 2008. Fixed rank kriging for very large spatial data sets. *Journal of the Royal Statistical Society Series B: Statistical Methodology* 70, 209–226.
- Datta, A., Banerjee, S., Finley, A.O., Gelfand, A.E., 2016. Hierarchical nearest-neighbor Gaussian process models for large geostatistical datasets. *Journal of the American Statistical Association* 111, 800–812.
- Diggle, Peter J., J.A.T., 1998. Model-based geostatistics. *Journal of the Royal Statistical Society Series C: Applied Statistics* 47, 299–350.
- Ferkingstad, E., Rue, H., 2015. Improving the inla approach for approximate bayesian inference for latent gaussian models. *Electronic Journal of Statistics* 9, 2706–2731.
- Flegal, J.M., Haran, M., Jones, G.L., 2008. Markov chain monte carlo: Can we trust the third significant figure? *Statistical Science* , 250–260.
- Fox, C.W., Roberts, S.J., 2012. A tutorial on variational bayesian inference. *Artificial intelligence review* 38, 85–95.

- Furrer, R., Genton, M.G., Nychka, D., 2006. Covariance tapering for interpolation of large spatial datasets. *Journal of Computational and Graphical Statistics* 15, 502–523.
- Garneau, S., Zanini, C.T., Schmidt, A.M., 2025. Semi-implicit approaches for large-scale bayesian spatial interpolation. *arXiv preprint arXiv:2510.19722* .
- Gneiting, T., Kleiber, W., Schlather, M., 2010. Matérn cross-covariance functions for multivariate random fields. *Journal of the American Statistical Association* 105, 1167–1177.
- Guan, Y., Haran, M., 2018. A computationally efficient projection-based approach for spatial generalized linear mixed models. *Journal of Computational and Graphical Statistics* 27, 701–714.
- Guo, F., Wang, X., Fan, K., Broderick, T., Dunson, D.B., 2016. Boosting variational inference. *arXiv preprint arXiv:1611.05559* .
- Hamelijnck, O., Wilkinson, W., Loppi, N., Solin, A., Damoulas, T., 2021. Spatio-temporal variational gaussian processes. *Advances in Neural Information Processing Systems* 34, 23621–23633.
- Han, S., Liao, X., Carin, L., 2013. Integrated non-factorized variational inference. *Advances in Neural Information Processing Systems* 26.
- Han, W., Yang, Y., 2019. Statistical inference in mean-field variational bayes. *arXiv preprint arXiv:1911.01525* .
- Haran, M., Hodges, J.S., Carlin, B.P., 2003. Accelerating computation in markov random field models for spatial data via structured mcmc. *Journal of Computational and Graphical Statistics* , 249–264.
- Higdon, D., 1998. A process-convolution approach to modelling temperatures in the north atlantic ocean. *Environmental and Ecological Statistics* 5, 173–190.
- Hoffman, M.D., Blei, D.M., Wang, C., Paisley, J., 2013. Stochastic variational inference. *Journal of Machine Learning Research* .
- Huszár, F., 2017. Variational inference using implicit distributions. *arXiv preprint arXiv:1702.08235* .

- Jaakkola, T.S., Jordan, M.I., 1997. A variational approach to bayesian logistic regression models and their extensions, in: Sixth International Workshop on Artificial Intelligence and Statistics, PMLR. pp. 283–294.
- Jordan, M.I., Ghahramani, Z., Jaakkola, T.S., Saul, L.K., 1999. An introduction to variational methods for graphical models. *Machine learning* 37, 183–233.
- Katzfuss, M., 2017. A multi-resolution approximation for massive spatial datasets. *Journal of the American Statistical Association* 112, 201–214.
- Kingma, D.P., Ba, J., 2014. Adam: A method for stochastic optimization. *arXiv preprint arXiv:1412.6980* .
- Kucukelbir, A., Tran, D., Ranganath, R., Gelman, A., Blei, D.M., 2017. Automatic differentiation variational inference. *Journal of machine learning research* 18, 1–45.
- Lee, B.S., Haran, M., 2022. Picar: An efficient extendable approach for fitting hierarchical spatial models. *Technometrics* 64, 187–198.
- Lee, B.S., Park, J., 2023. A scalable partitioned approach to model massive nonstationary non-gaussian spatial datasets. *Technometrics* 65, 105–116.
- Lee, J.H., Lee, B.S., 2024. A scalable variational bayes approach to fit high-dimensional spatial generalized linear mixed models. *arXiv preprint arXiv:2402.15705* .
- Li, Y., Turner, R.E., 2017. Gradient estimators for implicit models. *arXiv preprint arXiv:1705.07107* .
- Lim, J.N., Johansen, A., 2024. Particle semi-implicit variational inference. *Advances in Neural Information Processing Systems* 37, 123954–123990.
- Liu, J.S., Liu, J.S., 2001. Monte Carlo strategies in scientific computing. volume 10. Springer.
- Mescheder, L., Nowozin, S., Geiger, A., 2017. Adversarial variational bayes: Unifying variational autoencoders and generative adversarial networks, in: International conference on machine learning, PMLR. pp. 2391–2400.

- Mohamed, S., Lakshminarayanan, B., 2016. Learning in implicit generative models. arXiv preprint arXiv:1610.03483 .
- Mohammad-Djafari, A., Ayasso, H., 2009. Variational bayes and mean field approximations for markov field unsupervised estimation, in: 2009 IEEE International Workshop on Machine Learning for Signal Processing, IEEE. pp. 1–6.
- Nychka, D., Wikle, C., Royle, J.A., 2002. Multiresolution models for non-stationary spatial covariance functions. *Statistical Modelling* 2, 315–331.
- Parker, P.A., Holan, S.H., Janicki, R., 2022. Computationally efficient bayesian unit-level models for non-gaussian data under informative sampling with application to estimation of health insurance coverage. *The Annals of Applied Statistics* 16, 887–904.
- Polson, N.G., Scott, J.G., Windle, J., 2013. Bayesian inference for logistic models using pólya–gamma latent variables. *Journal of the American statistical Association* 108, 1339–1349.
- Popescu, M.C., Balas, V.E., Perescu-Popescu, L., Mastorakis, N., 2009. Multilayer perceptron and neural networks. *WSEAS Transactions on Circuits and Systems* 8, 579–588.
- Ranganath, R., Gerrish, S., Blei, D., 2014. Black box variational inference, in: *Artificial intelligence and statistics*, PMLR. pp. 814–822.
- Ranganath, R., Tran, D., Altosaar, J., Blei, D., 2016. Operator variational inference. *Advances in Neural Information Processing Systems* 29.
- Ranganath, R., Wang, C., David, B., Xing, E., 2013. An adaptive learning rate for stochastic variational inference, in: *International conference on machine learning*, PMLR. pp. 298–306.
- Redding, S.J., Rossi-Hansberg, E., 2017. Quantitative spatial economics. *Annual Review of Economics* 9, 21–58.
- Ren, Q., Banerjee, S., Finley, A.O., Hodges, J.S., 2011. Variational bayesian methods for spatial data analysis. *Computational statistics & data analysis* 55, 3197–3217.

- Rezende, D., Mohamed, S., 2015. Variational inference with normalizing flows, in: International conference on machine learning, PMLR. pp. 1530–1538.
- Rue, H., Martino, S., Chopin, N., 2009. Approximate Bayesian inference for latent Gaussian models by using integrated nested Laplace approximations. *Journal of the Royal Statistical Society: Series B (Statistical Methodology)* 71, 319–392.
- Rushton, G., 2003. Public health, gis, and spatial analytic tools. *Annual review of public health* 24, 43–56.
- Sengupta, A., Cressie, N., 2013. Hierarchical statistical modeling of big spatial datasets using the exponential family of distributions. *Spatial Statistics* 4, 14–44.
- Shi, J., Sun, S., Zhu, J., 2017. Implicit variational inference with kernel density ratio fitting. *arXiv preprint arXiv:1705.10119* .
- Song, J., Datta, A., 2025. Fast variational bayes for large spatial data. *arXiv preprint arXiv:2507.12251* .
- Tran, D., Ranganath, R., Blei, D., 2017. Hierarchical implicit models and likelihood-free variational inference. *Advances in Neural Information Processing Systems* 30.
- Tran, M.N., Nguyen, T.N., Dao, V.H., 2021. A practical tutorial on variational bayes. *arXiv preprint arXiv:2103.01327* .
- Wagner, H.H., Fortin, M.J., 2013. A conceptual framework for the spatial analysis of landscape genetic data. *Conservation Genetics* 14, 253–261.
- Wang, C., Blei, D.M., 2013. Variational inference in nonconjugate models. *The Journal of Machine Learning Research* 14, 1005–1031.
- Wikle, C.K., Berliner, L.M., Cressie, N., 1998. Hierarchical bayesian space-time models. *Environmental and ecological statistics* 5, 117–154.
- Wikle, C.K., Zammit-Mangion, A., Cressie, N., 2019. Spatio-temporal statistics with R. Chapman and Hall/CRC.

- Wu, G., 2018. Fast and scalable variational bayes estimation of spatial econometric models for gaussian data. *Spatial statistics* 24, 32–53.
- Yarger, D., Stoev, S., Hsing, T., 2023. Multivariate mat\`ern models—a spectral approach. *arXiv preprint arXiv:2309.02584* .
- Yin, M., Zhou, M., 2018. Semi-implicit variational inference, in: *International conference on machine learning*, PMLR. pp. 5660–5669.
- Zhou, Q., Li, J., 2020. Geo-spatial analysis in hydrology.
- Zilber, D., Katzfuss, M., 2021. Vecchia–laplace approximations of generalized gaussian processes for big non-gaussian spatial data. *Computational Statistics & Data Analysis* 153, 107081.
- Ziolkowski Jr., David, Lutmerding, M., Aponte, V., Hudson, M.A., 2022. 2022 release - North American breeding bird survey dataset (1966-2021). URL: <https://www.sciencebase.gov/catalog/item/625f151ed34e85fa62b7f926>, doi:10.5066/P97WAZE5.

Supplemental Information for
“A Scalable Variational Bayes Approach for
Fitting Non-Conjugate Spatial Generalized
Linear Mixed Models via Basis Expansions”

Hierarchical Structure in SIVI

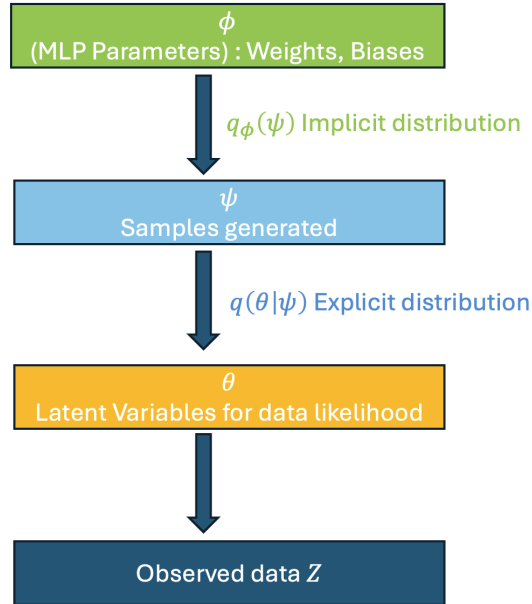


Figure S.1: ϕ denotes the weights and biases of the MLP, which define the implicit distribution, while ψ represents samples generated by the Multilayer Perceptron (MLP). These samples ψ are then used to estimate the latent variables and the observed data.

S.1. Simulation Study Results

We provide the simulation study results for the Bernoulli, Poisson, and Gaussian cases. Table S.1 provide an overview of the settings for ν and ϕ used in the main simulation study.

Table S.1: Simulation settings for smoothness parameter ν and spatial range parameter ϕ across different data types including gamma, negative binomial, binary, count and Gaussian.

Smoothness	Range	Data types
$\nu=0.5$	$\phi=0.1$	gamma, negative binomial, binary, count, and Gaussian
	$\phi=0.3$	gamma, negative binomial, binary, count, and Gaussian
$\nu=1.5$	$\phi=0.1$	gamma, negative binomial, binary, count, and Gaussian
	$\phi=0.3$	gamma, negative binomial, binary, count, and Gaussian

S.1.1. Data Model: Bernoulli Distribution

Table S.2 presents the AUC and walltime for Metropolis–Hastings (MH), Hamiltonian Monte Carlo (HMC), and Semi-Implicit Variational Inference (SIVI) applied to the binary data using the 50 leading eigenvectors. With the exception of the case $\nu = 1.5$ and $\phi = 0.3$, where all three methods produce identical results, the AUC from SIVI is slightly lower than that of MH and HMC. For example, when $\nu = 0.5$ and $\phi = 0.1$, both MH and HMC achieve an AUC of 0.756, requiring 1305.052 and 195.441 seconds of computation, respectively. In contrast, SIVI attains a comparable AUC of 0.752 while completing in only 21.840 seconds—representing speedups of approximately 59-fold relative to MH and 9-fold relative to HMC. Across the binary simulation studies, SIVI achieves computational gains of 45–59 times over MH and 6–9 times over HMC.

Figure S.2 further compares the posterior distributions of MH, HMC, and SIVI under the setting $\nu = 1.5$ and $\phi = 0.1$ for regression coefficients (β_1, β_2) , the variance component (σ^2) , and selected spatial random effects (δ_5, δ_7) . The results indicate that the three methods yield broadly similar posterior distributions.

Table S.2: Comparison of AUC, walltime (in seconds), and speedup for MH, HMC, and SIVI under different parameter settings for the Binary case.

	MH		HMC		SIVI		Speedup	
	AUC	Walltime	AUC	Walltime	AUC	Walltime	MH/SIVI	HMC/SIVI
Binary, $\nu = 0.5$								
$\phi = 0.1$	0.756	1305.052	0.756	195.441	0.752	21.840	59.755	8.949
$\phi = 0.3$	0.750	1308.432	0.750	186.651	0.749	24.719	52.933	7.551
Binary, $\nu = 1.5$								
$\phi = 0.1$	0.768	1242.841	0.768	181.665	0.763	23.768	52.290	7.643
$\phi = 0.3$	0.751	1256.131	0.751	184.890	0.751	27.401	45.843	6.748

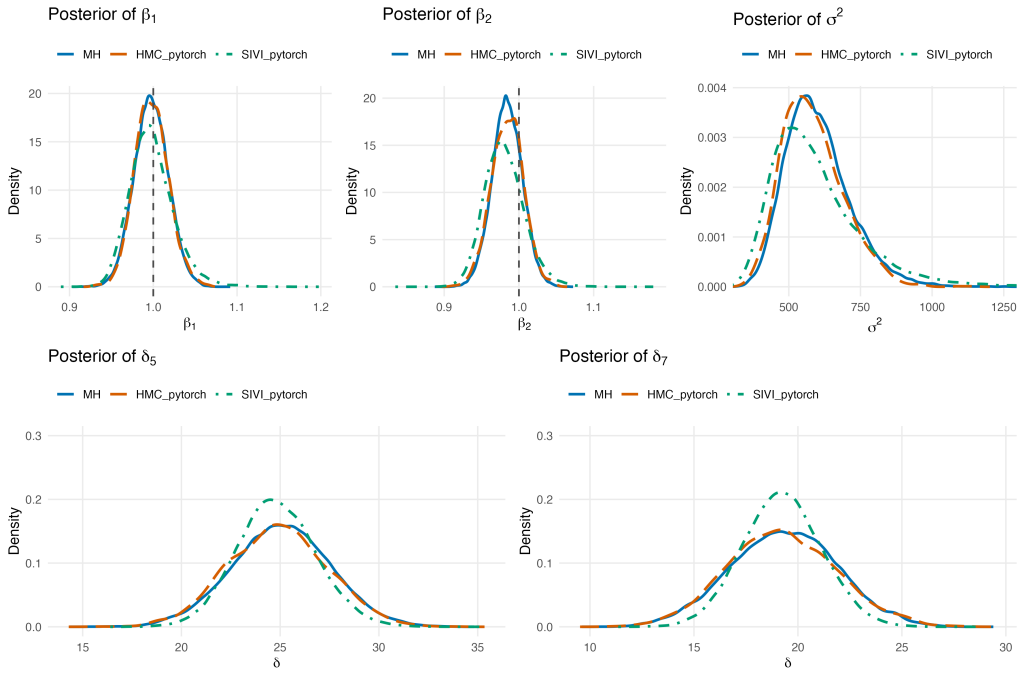


Figure S.2: Posterior density estimates of selected model parameters under three inference methods for the binary data when $\nu = 1.5$ and $\phi = 0.1$: Metropolis-Hastings (MH), Hamiltonian Monte Carlo (HMC), and Semi-Implicit Variational Inference (SIVI). Panels show results for regression coefficients (β_1, β_2), variance components (σ^2), and selected spatial random effects (δ_5, δ_7). Dashed vertical lines indicate the corresponding true parameter values where available. Overall, all three methods yield nearly indistinguishable posterior distributions, highlighting the accuracy of SIVI relative to MCMC-based approaches.

S.1.2. Data Model: Poisson Distribution

Table S.3 reports the RMSPE and walltime for Metropolis–Hastings (MH), Hamiltonian Monte Carlo (HMC), and Semi-Implicit Variational Inference (SIVI) applied to the count data using the 50 leading eigenvectors. In contrast to the binary case, SIVI achieves results that are virtually identical to those of MH and HMC. For example, when $\nu = 0.5$ and $\phi = 0.1$, all three methods yield an RMSPE of 1.374. However, the computational costs differ considerably: MH requires 1187.895 seconds, HMC requires 198.707 seconds, while SIVI completes in only 50.491 seconds, corresponding to speedups of approximately 23-fold relative to MH and 4-fold relative to HMC.

Figure S.3 further examines the posterior distributions of model parameters under the setting ($\nu = 0.5$, $\phi = 0.1$). The results show that regression coefficients (β_1, β_2), the variance component (σ^2), and spatial random effects (δ) are highly consistent across all three methods. Together, Figure S.3 and Table S.3 demonstrate that SIVI produces posterior distributions comparable to those from MH and HMC, while delivering substantial reductions in computation time.

Table S.3: Comparison of RMSPE, walltime (in seconds), and speedup for MH, HMC, and SIVI under different parameter settings for the count case.

	MH		HMC		SIVI		Speedup	
	RMSPE	Walltime	RMSPE	Walltime	RMSPE	Walltime	MH/SIVI	HMC/SIVI
Count, $\nu = 0.5$								
$\phi = 0.1$	1.374	1187.895	1.374	198.707	1.374	50.491	23.527	3.935
$\phi = 0.3$	1.489	1188.624	1.489	183.725	1.489	55.633	21.365	3.302
Count, $\nu = 1.5$								
$\phi = 0.1$	1.435	1304.939	1.435	184.019	1.450	53.754	24.276	3.423
$\phi = 0.3$	1.479	1341.094	1.479	184.804	1.480	57.300	23.405	3.225

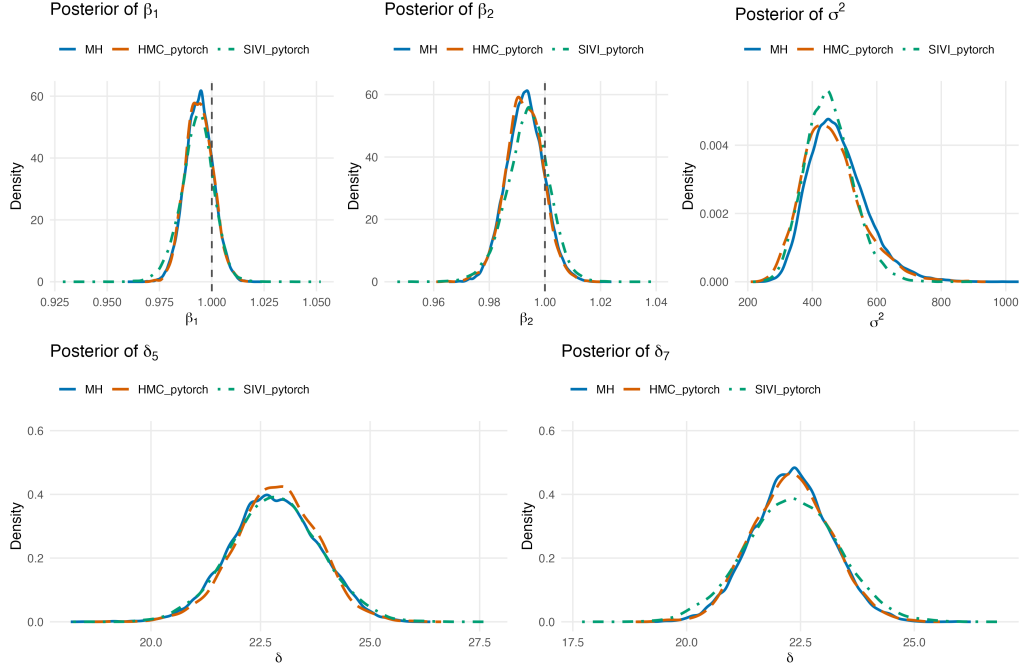


Figure S.3: Posterior density estimates of selected model parameters under three inference methods for the count data when $\nu = 0.5$ and $\phi = 0.1$: Metropolis-Hastings (MH), Hamiltonian Monte Carlo (HMC), and Semi-Implicit Variational Inference (SIVI). Panels show results for regression coefficients (β_1, β_2), variance components (σ^2), and selected spatial random effects (δ_5, δ_7). Dashed vertical lines indicate the corresponding true parameter values where available. Overall, all three methods yield nearly indistinguishable posterior distributions, highlighting the accuracy of SIVI relative to MCMC-based approaches.

S.1.3. Data Model: Gaussian Distribution

The Gaussian data case exhibits results consistent with those observed for the negative binomial, gamma, binary, and count models. Table S.4 reports the RMSPE and walltime for Metropolis–Hastings (MH), Hamiltonian Monte Carlo (HMC), and Semi-Implicit Variational Inference (SIVI). All three methods achieve an RMSPE of 1, yet their computational costs differ markedly: MH requires 650.205 seconds, HMC requires 62.720 seconds, while SIVI completes in only 23 seconds. This corresponds to speedups of approximately 28-fold relative to MH and 3-fold relative to HMC.

Figure S.4 compares the posterior distributions of model parameters under the setting $\nu = 0.5$ and $\phi = 0.1$. The results indicate that regression coefficients (β_1, β_2) , the variance component (σ^2) , and spatial random effects (δ) are nearly indistinguishable across MH, HMC, and SIVI.

Although variational inference methods, including SIVI, are often criticized for underestimating posterior variance (Blei and Jordan, 2006; Hoffman et al., 2013; Wu, 2018), our findings suggest that the proposed SIVI approach not only maintains predictive accuracy but also recovers posterior distributions that closely align with those from MCMC-based methods. This consistency holds across all data models considered—negative binomial, gamma, binary, count, and Gaussian—while providing substantial computational efficiency gains.

Table S.4: Comparison of RMSPE, walltime (in seconds), and speedup for MH, HMC, and SIVI under different parameter settings for the Gaussian case.

	MH		HMC		SIVI		Speedup	
	RMSPE	Walltime	RMSPE	Walltime	RMSPE	Walltime	MH/SIVI	HMC/SIVI
Gaussian, $\nu = 0.5$								
$\phi = 0.1$	1.000	650.205	1.000	62.720	1.000	23.143	28.095	2.710
$\phi = 0.3$	1.001	650.551	1.001	65.297	1.001	27.141	23.970	2.406
Gaussian, $\nu = 1.5$								
$\phi = 0.1$	1.000	684.511	1.000	60.818	1.000	26.325	26.003	2.310
$\phi = 0.3$	1.001	660.625	1.001	77.063	1.015	25.366	26.044	3.038

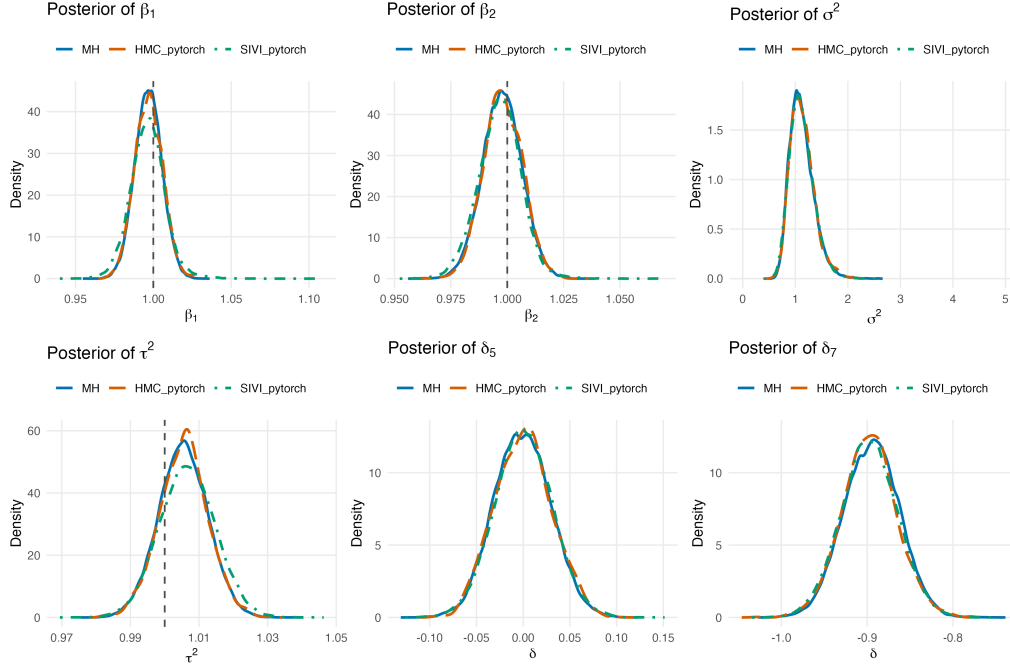


Figure S.4: Posterior density estimates of selected model parameters under three inference methods for the Gaussian data when $\nu = 0.5$ and $\phi = 0.1$: Metropolis-Hastings (MH), Hamiltonian Monte Carlo (HMC), and Semi-Implicit Variational Inference (SIVI). Panels show results for regression coefficients (β_1, β_2), variance components (σ^2, τ^2), and selected spatial random effects (δ_5, δ_7). Dashed vertical lines indicate the corresponding true parameter values where available. Overall, all three methods yield nearly indistinguishable posterior distributions, highlighting the accuracy of SIVI relative to MCMC-based approaches.

S.2. Derivation of ELBO Lower Bound in SIVI

SIVI incorporates an implicit mixing distribution $q_\phi(\boldsymbol{\psi})$, which distinguishes it from the existing literature that uses explicit variational distributions. In this study, we focus on the lower bound of the ELBO that arises from combining implicit and explicit distributions (Yin and Zhou, 2018). When the variational family includes an implicit distribution, the ELBO cannot be evaluated directly since the marginal variational density is intractable (Huszár, 2017; Mohamed and Lakshminarayanan, 2016). SIVI overcomes this by combining an explicit conditional distribution $q(\boldsymbol{\theta} \mid \boldsymbol{\psi})$ with an implicit mixing distribution $q_\phi(\boldsymbol{\psi})$. The resulting marginal variational density is

$$h_\phi(\boldsymbol{\theta}) = \mathbb{E}_{\boldsymbol{\psi} \sim q_\phi(\boldsymbol{\psi})} [q(\boldsymbol{\theta} \mid \boldsymbol{\psi})].$$

Using Jensen’s inequality and the convexity of the KL divergence (Cover, 1999), Yin and Zhou (2018) show that

$$\mathbb{E}_{\boldsymbol{\psi} \sim q_\phi(\boldsymbol{\psi})} \text{KL}(q(\boldsymbol{\theta} \mid \boldsymbol{\psi}) \parallel p(\boldsymbol{\theta})) \geq \text{KL}(h_\phi(\boldsymbol{\theta}) \parallel p(\boldsymbol{\theta})).$$

Applying this inequality to the ELBO yields the SIVI lower bound

$$\underline{\mathcal{L}} = \mathbb{E}_{\boldsymbol{\psi} \sim q_\phi(\boldsymbol{\psi})} \mathbb{E}_{\boldsymbol{\theta} \sim q(\boldsymbol{\theta} \mid \boldsymbol{\psi})} \left[\log \frac{p(\mathbf{Z}, \boldsymbol{\theta})}{q(\boldsymbol{\theta} \mid \boldsymbol{\psi})} \right],$$

which satisfies

$$\underline{\mathcal{L}} \leq \mathcal{L} = \mathbb{E}_{\boldsymbol{\theta} \sim h_\phi} \left[\log \frac{p(\mathbf{Z}, \boldsymbol{\theta})}{h_\phi(\boldsymbol{\theta})} \right].$$

The bound $\underline{\mathcal{L}}$ is computable because it depends only on the explicit density $q(\boldsymbol{\theta} \mid \boldsymbol{\psi})$, while the implicit mixing distribution $q_\phi(\boldsymbol{\psi})$ enters only through Monte Carlo sampling. Importantly, Yin and Zhou (2018) show that $\underline{\mathcal{L}}$ is asymptotically exact to the true ELBO; thereby allowing SIVI to retain the flexibility of implicit variational families while keeping ELBO optimization tractable (e.g, straightforward Monte Carlo estimation) of $\underline{\mathcal{L}}$.

S.3. General overview of SIVI Algorithm

Algorithm S.1 outlines SIVI when the explicit variational distribution is reparameterizable and the implicit mixing distribution is parameterized by a neural network. The algorithm requires the following inputs: the observed

data $\{\mathbf{Z}_i\}_{i=1}^N$, the joint likelihood $p(\mathbf{Z}, \boldsymbol{\theta})$, an explicit variational distribution $q(\boldsymbol{\theta} \mid \boldsymbol{\psi})$ with reparameterization $\boldsymbol{\theta} = f(\epsilon, \boldsymbol{\psi})$ where $\epsilon \sim p(\epsilon)$, and an implicit mixing distribution $q_\phi(\boldsymbol{\psi})$ defined through the neural network transformation $T_\phi(\epsilon)$ with randomness $\epsilon \sim q(\epsilon)$. The goal of the algorithm is to optimize the variational parameter ϕ , which corresponds to the weights and biases of the implicit neural network.

First, ϕ is initialized randomly. At each iteration, the surrogate lower bound \underline{L}_K is initialized to zero, and the step size η_t and the number of auxiliary samples K are specified. The implicit distribution $q_\phi(\boldsymbol{\psi})$ is then approximated by drawing random noise $\epsilon^{(k)} \sim q(\epsilon)$ and mapping it through the implicit neural network, yielding auxiliary samples $\boldsymbol{\psi}^{(k)} = T_\phi(\epsilon^{(k)})$.

To address the intractability of the implicit marginal distribution

$$h_\phi(\boldsymbol{\theta}) = \int q(\boldsymbol{\theta} \mid \boldsymbol{\psi}) q_\phi(\boldsymbol{\psi}) d\boldsymbol{\psi},$$

and specifically the challenge of evaluating $\log h_\phi(\boldsymbol{\theta})$ in the entropy term of the ELBO, the algorithm introduces an additional set of J auxiliary samples $\{\boldsymbol{\psi}_j\}_{j=1}^J$. For each $\boldsymbol{\psi}_j$, a reparameterized sample $\boldsymbol{\theta}_j = f(\tilde{\epsilon}_j, \boldsymbol{\psi}_j)$ is drawn with $\tilde{\epsilon}_j \sim p(\epsilon)$. The term $\log h_\phi(\boldsymbol{\theta}_j)$ is then approximated via Monte Carlo averaging over the K previously drawn auxiliary samples and the current $\boldsymbol{\psi}_j$, leading to the $(K + 1)$ -sample approximation:

$$\log h_\phi(\boldsymbol{\theta}_j) \approx \log \left(\frac{1}{K + 1} \left[\sum_{k=1}^K q(\boldsymbol{\theta}_j \mid \boldsymbol{\psi}^{(k)}) + q(\boldsymbol{\theta}_j \mid \boldsymbol{\psi}_j) \right] \right).$$

Including $\boldsymbol{\psi}_j$ among the averaging terms tightens the bound and reduces the risk of degeneracy in the variational approximation.

Finally, the surrogate lower bound \underline{L}_K is updated using contributions from the log-likelihood and prior terms, and the variational parameter ϕ is updated via gradient ascent with step size η_t . This iterative procedure continues until convergence, yielding the optimized ϕ that defines the implicit variational distribution. Figure 1 below provides an overview of the SIVI workflow of Algorithm S.1.

We use the lower bound $\underline{\mathcal{L}}$ of the ELBO \mathcal{L} to optimize our algorithm. Algorithm S.2 describes the semi-implicit variational inference (SIVI) procedure when the variational parameters ξ are updated for the explicit variational distribution $q(\mathbf{z} \mid \boldsymbol{\psi})$. Algorithm S.1 corresponds to the case where

the variational parameters ξ are not included. These algorithms can also be combined with subsampling techniques (Yin and Zhou, 2018). In our study, we employ Algorithm S.1 and do not use subsampling.

Algorithm S.1 Semi-Implicit Variational Inference (SIVI) when ξ are fixed (Yin and Zhou, 2018)

- 1: **Input:** Data $\{\mathbf{Z}_i\}_{1:N}$, joint likelihood $p(\mathbf{Z}, \boldsymbol{\theta})$, explicit variational distribution $q(\boldsymbol{\theta} \mid \boldsymbol{\psi})$ with reparameterization $\boldsymbol{\theta} = f(\epsilon, \boldsymbol{\psi})$, $\epsilon \sim p(\epsilon)$, implicit layer neural network $T_\phi(\epsilon)$ and source of randomness $q(\epsilon)$
 - 2: **Output:** Implicit variational parameter ϕ for the mixing distribution $q_\phi(\boldsymbol{\psi})$
 - 3: Initialize ϕ randomly
 - 4: **while** not converged **do**
 - 5: Set $\underline{L}_{K_t} = 0$ and η_t as step sizes, and $K_t \geq 0$ as a non-decreasing integer;
 - 6: Sample $\boldsymbol{\psi}^{(k)} = T_\phi(\epsilon^{(k)})$, $\epsilon^{(k)} \sim q(\epsilon)$ for $k = 1, \dots, K_t$;
 - 7: **for** $j = 1$ to J **do**
 - 8: Sample $\boldsymbol{\psi}_j = T_\phi(\epsilon_j)$, $\epsilon_j \sim q(\epsilon)$
 - 9: Sample $\boldsymbol{\theta}_j = f(\tilde{\epsilon}_j, \boldsymbol{\psi}_j)$, $\tilde{\epsilon}_j \sim p(\epsilon)$
 - 10:
$$\underline{L}_{K_t} \leftarrow \underline{L}_{K_t} + \frac{1}{J} \left\{ -\log \frac{1}{K_t + 1} \left[\sum_{k=1}^{K_t} q(\boldsymbol{\theta}_j \mid \boldsymbol{\psi}^{(k)}) + q(\boldsymbol{\theta}_j \mid \boldsymbol{\psi}_j) \right] \right. \\ \left. + \log p(\mathbf{Z} \mid \boldsymbol{\theta}_j) + \log p(\boldsymbol{\theta}_j) \right\}$$
 - 11: **end for**
 - 12: $t \leftarrow t + 1$
 - 13: $\phi \leftarrow \phi + \eta_t \nabla_\phi \underline{L}_{K_t} \left(\{\boldsymbol{\psi}^{(k)}\}_{1,K_t}, \{\boldsymbol{\psi}_j\}_{1,J}, \{\boldsymbol{\theta}_j\}_{1,J} \right)$
 - 14: **end while**
-

Algorithm S.2 Semi-Implicit Variational Inference (SIVI) when ξ are updated

(Yin and Zhou, 2018)

- 1: **Input:** Data $\{\mathbf{Z}_i\}_{1:N}$, joint likelihood $p(\mathbf{Z}, \boldsymbol{\theta})$, explicit variational distribution $q_\xi(\boldsymbol{\theta} \mid \boldsymbol{\psi})$ with reparameterization $\boldsymbol{\theta} = f(\epsilon, \xi, \boldsymbol{\psi})$, $\epsilon \sim p(\epsilon)$, implicit layer neural network $T_\phi(\epsilon)$ and source of randomness $q(\epsilon)$
 - 2: **Output:** Explicit Variational parameter ξ for the conditional distribution $q_\xi(\boldsymbol{\theta} \mid \boldsymbol{\psi})$,
implicit variational parameter ϕ for the mixing distribution $q_\phi(\boldsymbol{\psi})$
 - 3: Initialize ξ and ϕ randomly
 - 4: **while** not converged **do**
 - 5: Set $\underline{L}_{K_t} = 0$, ρ_t and η_t as step sizes, and $K_t \geq 0$ as a non-decreasing integer;
 - 6: Sample $\boldsymbol{\psi}^{(k)} = T_\phi(\epsilon^{(k)})$, $\epsilon^{(k)} \sim q(\epsilon)$ for $k = 1, \dots, K_t$;
 - 7: **for** $j = 1$ to J **do**
 - 8: Sample $\boldsymbol{\psi}_j = T_\phi(\epsilon_j)$, $\epsilon_j \sim q(\epsilon)$
 - 9: Sample $\boldsymbol{\theta}_j = f(\tilde{\epsilon}_j, \xi, \boldsymbol{\psi}_j)$, $\tilde{\epsilon}_j \sim p(\epsilon)$
 - 10:
$$\underline{L}_{K_t} \leftarrow \underline{L}_{K_t} + \frac{1}{J} \left\{ -\log \frac{1}{K_t + 1} \left[\sum_{k=1}^{K_t} q_\xi(\boldsymbol{\theta}_j \mid \boldsymbol{\psi}^{(k)}) + q_\xi(\boldsymbol{\theta}_j \mid \boldsymbol{\psi}_j) \right] \right. \\ \left. + \log p(\mathbf{Z} \mid \boldsymbol{\theta}_j) + \log p(\boldsymbol{\theta}_j) \right\}$$
 - 11: **end for**
 - 12: $t \leftarrow t + 1$
 - 13: $\xi \leftarrow \xi + \rho_t \nabla_\xi \underline{L}_{K_t} \left(\{\boldsymbol{\psi}^{(k)}\}_{1,K_t}, \{\boldsymbol{\psi}_j\}_{1,J}, \{\boldsymbol{\theta}_j\}_{1,J} \right)$
 - 14: $\phi \leftarrow \phi + \eta_t \nabla_\phi \underline{L}_{K_t} \left(\{\boldsymbol{\psi}^{(k)}\}_{1,K_t}, \{\boldsymbol{\psi}_j\}_{1,J}, \{\boldsymbol{\theta}_j\}_{1,J} \right)$
 - 15: **end while**
-

S.4. Sensitivity Analysis for Stopping Criteria in SIVI

In this section, we examine the effect of different stopping criteria (10^{-1} , 10^{-3} , and 10^{-4}) on SIVI performance. For each setting, we report RMSPE, walltime (seconds), and speedup for MH, HMC, and SIVI across all data types considered - negative binomial, gamma, Bernoulli, Poisson, and Gaussian.

S.4.1. Tables by using stopping criteria ($1e-1$) for SIVI

Table S.5: Comparison of RMSPE, walltime (in seconds), and speedup for MH, HMC, and SIVI under different parameter settings for the Negative Binomial (NB) case, when we use the 10^{-1} stopping criteria for SIVI.

	MH		HMC		SIVI		Speedup	
	RMSPE	Walltime	RMSPE	Walltime	RMSPE	Walltime	MH/SIVI	HMC/SIVI
NB, $\nu = 0.5$								
$\phi = 0.1$	3.473	3194.339	3.473	138.831	3.475	38.054	83.943	3.648
$\phi = 0.3$	3.930	3308.680	3.930	148.911	3.938	34.994	94.550	4.255
NB, $\nu = 1.5$								
$\phi = 0.1$	3.971	3162.185	3.971	141.780	3.981	35.941	87.982	3.945
$\phi = 0.3$	3.887	3334.172	3.887	168.685	3.895	36.397	91.606	4.635

Table S.6: Comparison of RMSPE, walltime (in seconds), and speedup for MH, HMC, and SIVI under different parameter settings for the Gamma case, when we use the 10^{-1} stopping criteria for SIVI.

	MH		HMC		SIVI		Speedup	
	RMSPE	Walltime	RMSPE	Walltime	RMSPE	Walltime	MH/SIVI	HMC/SIVI
Gamma, $\nu = 0.5$								
$\phi = 0.1$	3.945	4291.942	3.945	122.830	3.961	12.702	337.907	9.670
$\phi = 0.3$	3.855	4071.220	3.855	129.538	3.869	11.801	345.002	10.977
Gamma, $\nu = 1.5$								
$\phi = 0.1$	4.614	4204.997	4.614	116.045	4.616	11.918	352.824	9.737
$\phi = 0.3$	3.559	4577.599	3.559	138.682	3.560	11.973	382.322	11.583

Table S.7: Comparison of RMSPE, walltime (in seconds), and speedup for MH, HMC, and SIVI under different parameter settings for the Count case, when we use the 10^{-1} stopping criteria for SIVI.

	MH		HMC		SIVI		Speedup	
	RMSPE	Walltime	RMSPE	Walltime	RMSPE	Walltime	MH/SIVI	HMC/SIVI
Count, $\nu = 0.5$								
$\phi = 0.1$	1.374	1187.895	1.374	218.930	1.382	23.220	51.158	9.428
$\phi = 0.3$	1.489	1188.624	1.489	203.563	1.494	27.544	43.153	7.390
Count, $\nu = 1.5$								
$\phi = 0.1$	1.435	1304.939	1.435	201.499	1.502	25.905	50.375	7.778
$\phi = 0.3$	1.479	1341.094	1.479	205.189	1.502	28.665	46.785	7.158

Table S.8: Comparison of AUC, walltime (in seconds), and speedup for MH, HMC, and SIVI under different parameter settings for the Binary case, when we use the 10^{-1} stopping criteria for SIVI.

	MH		HMC		SIVI		Speedup	
	AUC	Walltime	AUC	Walltime	AUC	Walltime	MH/SIVI	HMC/SIVI
Binary, $\nu = 0.5$								
$\phi = 0.1$	0.756	1305.052	0.756	216.202	0.735	9.070	143.891	23.838
$\phi = 0.3$	0.750	1308.432	0.750	227.728	0.731	9.620	136.012	23.673
Binary, $\nu = 1.5$								
$\phi = 0.1$	0.768	1242.841	0.768	181.665	0.763	23.768	52.290	7.643
$\phi = 0.3$	0.751	1256.131	0.751	184.890	0.751	27.401	45.843	6.748

Table S.9: Comparison of RMSPE, walltime (in seconds), and speedup for MH, HMC, and SIVI under different parameter settings for the Gaussian case, when we use the 10^{-1} stopping criteria for SIVI.

	MH		HMC		SIVI		Speedup	
	RMSPE	Walltime	RMSPE	Walltime	RMSPE	Walltime	MH/SIVI	HMC/SIVI
Gaussian, $\nu = 0.5$								
$\phi = 0.1$	1.000	650.205	1.000	62.124	1.005	11.796	55.122	5.267
$\phi = 0.3$	1.001	650.551	1.001	66.697	1.002	13.270	49.026	5.026
Gaussian, $\nu = 1.5$								
$\phi = 0.1$	1.000	1144.796	1.000	60.007	1.000	12.993	88.112	4.619
$\phi = 0.3$	1.001	660.625	1.001	76.154	1.015	11.907	55.481	6.396

Table S.10: Walltime quantiles (25%, 50%, 75%) for MH, HMC, and SIVI with SIVI stopping criterion $\epsilon = 10^{-1}$, and corresponding speedups (MH/SIVI, HMC/SIVI). Red values highlight median speedups.

	MH			HMC			SIVI			Speedup (MH/SIVI)			Speedup (HMC/SIVI)		
	25%	50%	75%	25%	50%	75%	25%	50%	75%	25%	50%	75%	25%	50%	75%
NB															
$\nu = 0.5$															
$\phi = 0.1$	3038.053	3205.406	3332.122	117.461	129.722	153.758	29.320	38.406	45.472	103.618	83.461	73.279	4.006	3.378	3.381
$\phi = 0.3$	3205.791	3337.000	3431.428	128.285	138.807	167.047	26.425	33.084	44.680	121.317	100.864	76.800	4.855	4.196	3.739
$\nu = 1.5$															
$\phi = 0.1$	3041.410	3165.704	3265.998	119.776	138.726	159.894	27.977	34.950	42.384	108.711	90.578	77.057	4.281	3.969	3.773
$\phi = 0.3$	3212.261	3385.727	3450.251	152.501	162.734	182.837	26.386	33.917	47.816	121.743	99.822	72.157	5.780	4.798	3.824
Gamma															
$\nu = 0.5$															
$\phi = 0.1$	3435.886	3540.562	3684.057	105.957	122.399	140.450	8.334	12.532	16.276	412.273	282.522	226.349	12.714	9.767	8.629
$\phi = 0.3$	3216.671	3337.640	3478.441	111.208	130.591	148.576	6.741	10.674	15.445	477.180	312.689	225.215	16.497	12.234	9.620
$\nu = 1.5$															
$\phi = 0.1$	3287.160	3479.287	3607.622	95.533	116.644	133.472	7.110	12.225	15.106	462.350	284.596	238.824	13.436	9.541	8.836
$\phi = 0.3$	2975.072	3150.037	3357.022	121.353	139.674	153.938	6.781	10.831	17.114	438.749	290.834	196.159	17.896	12.896	8.995
Binary															
$\nu = 0.5$															
$\phi = 0.1$	1102.228	1361.181	1534.596	207.740	213.407	226.810	3.516	7.821	13.080	313.489	174.042	117.324	59.084	27.286	17.340
$\phi = 0.3$	1100.464	1371.999	1527.190	206.923	221.621	240.509	3.989	8.994	13.774	275.875	152.546	110.875	51.873	24.641	17.461
$\nu = 1.5$															
$\phi = 0.1$	1060.812	1158.577	1504.216	176.949	179.800	184.317	15.382	27.420	31.645	68.965	42.253	47.534	11.504	6.557	5.825
$\phi = 0.3$	1048.858	1260.038	1503.935	179.101	182.640	189.276	18.710	26.934	34.497	56.059	46.782	43.596	9.572	6.781	5.487
Count															
$\nu = 0.5$															
$\phi = 0.1$	1043.119	1199.590	1228.619	201.462	220.268	236.339	16.670	23.314	27.582	62.575	51.454	44.544	12.085	9.448	8.569
$\phi = 0.3$	1045.639	1185.762	1239.167	186.200	207.146	221.766	18.964	24.873	34.772	55.139	47.673	35.637	9.819	8.328	6.378
$\nu = 1.5$															
$\phi = 0.1$	1089.074	1367.412	1515.595	175.381	196.032	220.526	16.896	27.213	34.846	64.458	50.248	43.494	10.380	7.204	6.329
$\phi = 0.3$	1100.422	1461.657	1525.157	176.261	203.580	225.811	18.714	29.923	38.702	58.802	48.847	39.408	9.419	6.803	5.835
Gaussian															
$\nu = 0.5$															
$\phi = 0.1$	560.900	678.775	692.222	51.565	56.302	72.026	8.763	12.609	15.088	64.008	53.833	45.879	5.884	4.465	4.774
$\phi = 0.3$	559.832	679.687	691.575	62.513	66.317	72.021	8.754	13.067	16.020	63.952	52.016	43.169	7.141	5.075	4.496
$\nu = 1.5$															
$\phi = 0.1$	672.899	681.511	688.272	57.459	66.417	80.091	10.313	13.677	15.635	65.248	49.829	44.021	5.572	4.856	5.123
$\phi = 0.3$	645.736	681.685	688.288	66.718	75.579	84.850	8.090	12.135	15.854	79.814	56.175	43.414	8.247	6.228	5.352

S.4.2. Tables by using stopping criteria ($1e-3$) for SIVI

Table S.11: Comparison of RMSPE, walltime (in seconds), and speedup for MH, HMC, and SIVI under different parameter settings for the Negative Binomial (NB) case, when we use the 10^{-3} stopping criteria for SIVI.

	MH		HMC		SIVI		Speedup	
	RMSPE	Walltime	RMSPE	Walltime	RMSPE	Walltime	MH/SIVI	HMC/SIVI
NB, $\nu = 0.5$								
$\phi = 0.1$	3.473	3194.339	3.473	142.706	3.473	126.521	25.247	1.128
$\phi = 0.3$	3.930	3308.680	3.930	152.007	3.930	146.967	22.513	1.034
NB, $\nu = 1.5$								
$\phi = 0.1$	3.971	3162.185	3.971	140.109	3.973	135.374	23.359	1.035
$\phi = 0.3$	3.887	3334.172	3.887	169.582	3.887	129.575	25.732	1.309

Table S.12: Comparison of RMSPE, walltime (in seconds), and speedup for MH, HMC, and SIVI under different parameter settings for the Gamma case, when we use the 10^{-3} stopping criteria for SIVI.

	MH		HMC		SIVI		Speedup	
	RMSPE	Walltime	RMSPE	Walltime	RMSPE	Walltime	MH/SIVI	HMC/SIVI
Gamma, $\nu = 0.5$								
$\phi = 0.1$	4.614	4204.997	4.614	121.774	4.614	60.760	69.206	2.004
$\phi = 0.3$	3.559	4577.599	3.559	145.113	3.559	88.178	51.913	1.646
Gamma, $\nu = 1.5$								
$\phi = 0.1$	3.945	4291.942	3.945	127.911	3.944	60.680	70.731	2.108
$\phi = 0.3$	3.855	4071.220	3.855	137.453	3.855	62.252	65.399	2.208

Table S.13: Comparison of AUC, walltime (in seconds), and speedup for MH, HMC, and SIVI under different parameter settings for the Binary case, when we use the 10^{-3} stopping criteria for SIVI.

	MH		HMC		SIVI		Speedup	
	AUC	Walltime	AUC	Walltime	AUC	Walltime	MH/SIVI	HMC/SIVI
Binary, $\nu = 0.5$								
$\phi = 0.1$	0.756	1305.052	0.756	239.870	0.756	72.414	18.022	3.312
$\phi = 0.3$	0.750	1308.432	0.750	226.196	0.749	63.186	20.708	3.580
Binary, $\nu = 1.5$								
$\phi = 0.1$	0.768	1242.841	0.768	235.282	0.766	69.785	17.810	3.372
$\phi = 0.3$	0.751	1256.131	0.751	228.975	0.751	76.491	16.422	2.993

Table S.14: Comparison of RMSPE, walltime (in seconds), and speedup for MH, HMC, and SIVI under different parameter settings for the Count case, when we use the 10^{-3} stopping criteria for SIVI.

	MH		HMC		SIVI		Speedup	
	RMSPE	Walltime	RMSPE	Walltime	RMSPE	Walltime	MH/SIVI	HMC/SIVI
Count, $\nu = 0.5$								
$\phi = 0.1$	1.374	1187.895	1.374	203.727	1.374	79.767	14.892	2.554
$\phi = 0.3$	1.489	1188.624	1.489	199.552	1.490	81.929	14.508	2.436
Count, $\nu = 1.5$								
$\phi = 0.1$	1.435	1304.939	1.435	253.268	1.437	116.549	11.196	2.173
$\phi = 0.3$	1.479	1341.094	1.479	250.507	1.481	108.057	12.411	2.318

Table S.15: Comparison of RMSPE, walltime (in seconds), and speedup for MH, HMC, and SIVI under different parameter settings for the Gaussian case, when we use the 10^{-3} stopping criteria for SIVI.

	MH		HMC		SIVI		Speedup	
	RMSPE	Walltime	RMSPE	Walltime	RMSPE	Walltime	MH/SIVI	HMC/SIVI
Gaussian, $\nu = 0.5$								
$\phi = 0.1$	1.000	650.205	1.000	72.100	1.000	44.465	14.623	1.621
$\phi = 0.3$	1.001	650.551	1.001	78.032	1.001	59.823	10.875	1.304
Gaussian, $\nu = 1.5$								
$\phi = 0.1$	1.000	684.511	1.000	60.907	1.000	42.352	16.162	1.438
$\phi = 0.3$	1.001	660.625	1.001	78.869	1.001	68.319	9.670	1.154

Table S.16: Walltime quantiles (25%, 50%, 75%) for MH, HMC, and SIVI with SIVI stopping criterion $\epsilon = 10^{-3}$, and corresponding speedups (MH/SIVI, HMC/SIVI). Red values highlight median speedups.

	MH			HMC			SIVI			Speedup (MH/SIVI)			Speedup (HMC/SIVI)		
	25%	50%	75%	25%	50%	75%	25%	50%	75%	25%	50%	75%	25%	50%	75%
NB															
$\nu = 0.5$															
$\phi = 0.1$	3038.053	3205.406	3332.122	121.477	134.756	159.281	58.569	68.310	86.513	51.871	46.924	38.516	2.074	1.973	1.841
$\phi = 0.3$	3205.791	3337.000	3431.428	124.543	133.702	160.183	51.481	79.814	98.385	62.272	41.809	34.878	2.419	1.675	1.628
$\nu = 1.5$															
$\phi = 0.1$	3041.410	3165.704	3265.998	106.224	123.283	142.447	61.417	78.272	92.491	49.521	40.445	35.312	1.730	1.575	1.540
$\phi = 0.3$	3212.261	3385.727	3450.251	136.075	146.063	166.988	57.535	72.337	89.648	55.831	46.805	38.487	2.365	2.019	1.863
Gamma															
$\nu = 0.5$															
$\phi = 0.1$	3435.886	3540.562	3684.057	105.796	122.750	139.434	18.115	27.315	41.319	189.667	129.621	89.161	5.840	4.494	3.375
$\phi = 0.3$	3216.671	3337.640	3478.441	110.334	121.261	147.809	18.892	33.153	37.471	170.267	100.675	73.430	5.837	3.959	3.120
$\nu = 1.5$															
$\phi = 0.1$	3287.160	3479.287	3607.622	93.948	109.456	129.891	22.993	36.281	44.389	142.963	95.899	81.272	4.086	3.017	2.926
$\phi = 0.3$	2975.072	3150.037	3357.022	112.922	131.158	144.769	27.034	34.083	50.282	110.049	92.424	66.764	4.177	3.848	2.879
Binary															
$\nu = 0.5$															
$\phi = 0.1$	1102.228	1361.181	1534.596	178.892	184.339	195.206	14.728	22.249	29.604	74.840	61.180	51.837	12.147	8.285	6.594
$\phi = 0.3$	1100.464	1371.999	1527.190	179.067	184.389	191.079	17.481	26.021	33.474	62.952	52.727	45.623	12.743	7.086	5.708
$\nu = 1.5$															
$\phi = 0.1$	1060.812	1158.577	1504.216	176.950	179.799	184.318	15.382	27.420	31.645	68.962	42.253	47.535	11.503	6.557	5.825
$\phi = 0.3$	1048.858	1260.038	1503.935	179.101	182.640	189.276	18.710	26.934	34.497	56.058	46.782	43.596	9.572	6.781	5.487
Count															
$\nu = 0.5$															
$\phi = 0.1$	1043.119	1199.590	1228.619	183.375	203.553	221.501	53.751	90.772	106.684	19.407	13.215	11.516	4.197	13.215	11.516
$\phi = 0.3$	1045.639	1185.762	1239.167	184.518	203.658	215.995	58.996	91.017	107.471	17.724	13.028	11.530	4.172	13.028	11.530
$\nu = 1.5$															
$\phi = 0.1$	1089.074	1367.412	1515.595	206.664	255.867	302.661	81.532	108.682	150.878	13.358	12.562	10.405	3.834	12.562	10.405
$\phi = 0.3$	1100.422	1461.657	1525.157	215.875	254.626	278.025	78.812	107.563	145.243	13.963	13.589	10.501	3.639	13.589	10.501
Gaussian															
$\nu = 0.5$															
$\phi = 0.1$	560.900	678.775	692.222	61.237	67.676	81.171	28.500	41.047	60.140	19.681	16.536	11.510	2.149	1.649	1.350
$\phi = 0.3$	559.822	679.687	692.743	67.691	74.976	89.590	33.497	50.201	80.250	16.712	13.539	8.632	2.021	1.493	1.116
$\nu = 1.5$															
$\phi = 0.1$	672.899	684.511	688.272	50.823	56.334	70.857	28.423	37.229	49.793	23.675	18.387	13.823	1.788	1.513	1.423
$\phi = 0.3$	645.736	681.685	688.288	68.573	75.666	90.374	40.147	63.436	93.278	16.084	10.746	7.379	1.708	1.193	0.969

S.4.3. Tables by using stopping criteria ($1e-4$) for SIVI

Table S.17: Comparison of RMSPE, walltime (in seconds), and speedup for MH, HMC, and SIVI under different parameter settings for the Negative Binomial (NB) case, when we use the 10^{-4} stopping criteria for SIVI.

	MH		HMC		SIVI		Speedup	
	RMSPE	Walltime	RMSPE	Walltime	RMSPE	Walltime	MH/SIVI	HMC/SIVI
NB, $\nu = 0.5$								
$\phi = 0.1$	3.473	3194.339	3.473	127.039	3.473	124.081	25.744	1.024
$\phi = 0.3$	3.930	3308.680	3.930	136.123	3.930	144.391	22.915	0.943
NB, $\nu = 1.5$								
$\phi = 0.1$	3.971	3162.185	3.971	147.604	3.972	157.521	20.075	0.937
$\phi = 0.3$	3.887	3334.172	3.887	159.560	3.887	149.573	22.291	1.067

Table S.18: Comparison of RMSPE, walltime (in seconds), and speedup for MH, HMC, and SIVI under different parameter settings for the Gamma case, when we use the 10^{-4} stopping criteria for SIVI.

	MH		HMC		SIVI		Speedup	
	RMSPE	Walltime	RMSPE	Walltime	RMSPE	Walltime	MH/SIVI	HMC/SIVI
Gamma, $\nu = 0.5$								
$\phi = 0.1$	3.945	4291.942	3.945	112.035	3.945	48.140	89.156	2.327
$\phi = 0.3$	3.855	4071.220	3.855	118.661	3.855	63.923	63.689	1.856
Gamma, $\nu = 1.5$								
$\phi = 0.1$	4.614	4204.997	4.614	120.981	4.614	54.001	77.868	2.240
$\phi = 0.3$	3.559	4577.599	3.559	145.155	3.559	81.555	56.129	1.780

Table S.19: Comparison of RMSPE, walltime (in seconds), and speedup for MH, HMC, and SIVI under different parameter settings for the Count case, when we use the 10^{-4} stopping criteria for SIVI.

	MH		HMC		SIVI		Speedup	
	RMSPE	Walltime	RMSPE	Walltime	RMSPE	Walltime	MH/SIVI	HMC/SIVI
Count, $\nu = 0.5$								
$\phi = 0.1$	1.374	1187.895	1.374	198.726	1.374	76.099	15.610	2.611
$\phi = 0.3$	1.489	1188.624	1.489	183.361	1.489	82.873	14.343	2.213
Count, $\nu = 1.5$								
$\phi = 0.1$	1.435	1304.939	1.435	185.134	1.450	75.955	17.181	2.437
$\phi = 0.3$	1.479	1341.094	1.479	185.299	1.480	84.551	15.861	2.192

Table S.20: Comparison of AUC, walltime (in seconds), and speedup for MH, HMC, and SIVI under different parameter settings for the Binary case, when we use the 10^{-4} stopping criteria for SIVI.

	MH		HMC		SIVI		Speedup	
	AUC	Walltime	AUC	Walltime	AUC	Walltime	MH/SIVI	HMC/SIVI
Binary, $\nu = 0.5$								
$\phi = 0.1$	0.756	1305.052	0.756	221.527	0.756	58.770	22.206	3.769
$\phi = 0.3$	0.750	1308.432	0.750	244.570	0.750	66.535	19.665	3.676
Binary, $\nu = 1.5$								
$\phi = 0.1$	0.768	1242.841	0.768	181.665	0.763	23.768	52.290	7.643
$\phi = 0.3$	0.751	1256.131	0.751	184.890	0.751	27.401	45.843	6.748

Table S.21: Comparison of RMSPE, walltime (in seconds), and speedup for MH, HMC, and SIVI under different parameter settings for the Gaussian case, when we use the 10^{-4} stopping criteria for SIVI.

	MH		HMC		SIVI		Speedup	
	RMSPE	Walltime	RMSPE	Walltime	RMSPE	Walltime	MH/SIVI	HMC/SIVI
Gaussian, $\nu = 0.5$								
$\phi = 0.1$	1.000	650.205	1.000	73.118	1.000	38.826	16.747	1.883
$\phi = 0.3$	1.001	650.551	1.001	75.269	1.001	49.616	13.112	1.517
Gaussian, $\nu = 1.5$								
$\phi = 0.1$	1.000	684.511	1.000	67.510	1.000	45.505	15.043	1.484
$\phi = 0.3$	1.001	660.625	1.001	76.521	1.015	55.625	11.876	1.376

Table S.22: Walltime quantiles (25%, 50%, 75%) for MH, HMC, and SIVI with SIVI stopping criterion $\epsilon = e^{-4}$, and corresponding speedups (MH/SIVI, HMC/SIVI). Red values highlight median speedups.

	MH			HMC			SIVI			Speedup (MH/SIVI)			Speedup (HMC/SIVI)		
	25%	50%	75%	25%	50%	75%	25%	50%	75%	25%	50%	75%	25%	50%	75%
NB															
$\nu = 0.5$															
$\phi = 0.1$	3038.053	3205.406	3332.122	107.641	120.831	140.437	83.232	106.617	148.620	36.507	30.065	22.420	1.293	1.133	0.945
$\phi = 0.3$	3205.791	3337.000	3431.428	126.542	153.687	182.183	84.014	126.849	182.183	38.158	26.307	18.835	1.402	0.998	0.844
$\nu = 1.5$															
$\phi = 0.1$	3041.410	3165.704	3265.998	123.971	144.374	167.344	99.140	146.179	188.494	30.678	21.656	17.327	1.250	0.988	0.888
$\phi = 0.3$	3212.261	3385.727	3450.251	139.664	151.710	174.620	81.366	125.747	180.512	39.479	26.925	19.114	1.716	1.206	0.967
Gamma															
$\nu = 0.5$															
$\phi = 0.1$	3435.886	3540.562	3684.057	112.361	127.280	139.434	36.227	47.815	54.909	94.844	74.047	67.094	2.665	2.350	2.318
$\phi = 0.3$	3216.671	3337.640	3478.441	121.122	135.219	148.576	35.844	64.731	80.045	89.741	51.562	43.456	2.382	1.871	1.689
$\nu = 1.5$															
$\phi = 0.1$	3287.160	3479.287	3607.622	100.009	123.612	138.951	33.891	53.893	68.950	96.991	64.559	52.322	2.951	2.286	2.015
$\phi = 0.3$	2975.072	3150.037	3357.022	126.366	146.534	165.024	51.430	76.504	119.755	57.847	41.175	28.032	2.462	1.915	1.378
Binary															
$\nu = 0.5$															
$\phi = 0.1$	1102.228	1361.181	1534.596	220.746	220.937	232.028	36.550	49.865	69.015	30.157	27.297	22.236	5.971	4.431	3.362
$\phi = 0.3$	1100.464	1371.999	1527.190	243.403	256.529	256.529	45.188	58.132	81.778	24.353	23.601	18.657	5.391	4.187	3.363
$\nu = 1.5$															
$\phi = 0.1$	1060.812	1158.577	1504.216	176.959	179.799	184.318	15.382	27.420	31.645	68.962	42.253	47.535	11.503	6.557	5.825
$\phi = 0.3$	1048.858	1260.038	1503.935	179.101	182.640	189.276	18.710	26.934	34.497	56.058	46.782	43.596	9.572	6.781	5.487
Count															
$\nu = 0.5$															
$\phi = 0.1$	1043.119	1199.590	1228.619	183.542	199.553	215.915	58.354	81.956	95.518	17.876	14.637	12.863	17.876	14.637	12.863
$\phi = 0.3$	1045.639	1185.762	1239.167	169.421	184.509	199.852	63.100	89.074	108.949	16.571	13.312	11.374	16.571	13.312	11.374
$\nu = 1.5$															
$\phi = 0.1$	1089.074	1367.412	1515.595	159.561	180.962	202.700	55.787	80.965	106.868	19.522	16.889	14.182	19.522	16.889	14.182
$\phi = 0.3$	1100.422	1461.657	1525.157	159.815	181.326	205.011	59.847	87.139	108.912	18.387	16.774	14.004	18.387	16.774	14.004
Gaussian															
$\nu = 0.5$															
$\phi = 0.1$	560.900	678.775	692.222	61.827	68.941	84.581	28.449	36.796	49.246	19.716	18.447	14.056	2.173	1.861	1.718
$\phi = 0.3$	559.832	679.687	691.575	66.164	72.995	84.423	27.033	46.384	61.083	20.712	14.647	11.324	2.448	1.870	1.383
$\nu = 1.5$															
$\phi = 0.1$	672.899	684.511	688.272	51.203	61.916	77.210	34.893	42.841	54.852	19.285	15.978	12.548	1.467	1.457	1.408
$\phi = 0.3$	645.736	681.685	688.288	65.757	70.681	87.197	34.525	51.577	70.540	18.704	13.217	9.757	1.905	1.370	1.236